ORIGINAL PAPER

Cyclic Frictional Responses of Planar Joints Under Cyclic Normal Load Conditions: Laboratory Tests and Numerical Simulations

Wengang Dang[1] · Heinz Konietzky[2] · Thomas Frühwirt[2] · Martin Herbst[2]

Abstract
An accurate quantification of the frictional behaviour of joints under cyclic normal load conditions during the cyclic shear process is important to characterize the joint and fault interactions during earthquakes and rock bursts. We conducted experimental studies and numerical simulations to investigate the cyclic frictional responses of planar joints subjected to cyclic changes of normal loads. Experiments were conducted on artificial rock-like planar joints using a large shear box device (GS-1000), with different vertical and horizontal impact frequencies, vertical impact load amplitudes, horizontal shear displacement amplitudes, and normal load levels. The average normal displacement of the upper block increased with decreasing normal load and decreased with increasing normal load during each cycle. The normal displacement decreased gradually with increasing number of shear cycles due to damage to the micro-asperities at the contact surface. Shear force and the apparent coefficient of friction ($k = F_{\text{Shear}}/F_{\text{Normal}}$) changed cyclically with a change in shear direction, where k followed a square wave curve with the same peak value at the stable shear stage. The cyclic normal load amplitudes, horizontal shear displacement amplitudes, cyclic normal load frequencies, cyclic horizontal shear frequencies, and static normal force levels had little influence on the peak values of k. Numerical simulations proved that the spatial movement pattern of the loading plate and upper block of the specimen rotated clockwise or anti-clockwise at different shear displacements. Due to the rotation of the upper block, shear and normal stresses distributed at the contact surface were inhomogeneous, which generated a stress gradient along the interface. Consequently, the samples were damaged at the two edges due to the high local stresses. Finally, a mathematical equation is proposed, which can be used for predicting the shear strength of planar joints under cyclic changes of shear velocity and normal load.

Keywords Cyclic normal load · Cyclic shear load · Numerical simulation · Planar joints · Apparent coefficient of friction

List of Symbols

F_N [kN]   Total normal load
F_s [kN]   Quasi-static normal load
F_d [kN]   Amplitude of superimposed dynamic normal load
F_{sd} [kN]   Impact normal load
σ_n [MPa]   Normal stress
τ [MPa]   Shear stress
v [mm/min]   Shear velocity
S [m²]   Nominal area of the shear plane
f_h [Hz]   Cyclic horizontal shear frequency
f_v [Hz]   Cyclic normal load impact frequency
t [s]   Time
Δt [s]   Time shift
k [–]   Apparent coefficient of friction
K [–]   Peak value of the apparent coefficient of friction
u_{max} [mm]   Amplitude of shear displacement
u_s [mm]   Shear displacement
n [–]   Number of Fourier series elements
$u_{n(a)}$ [mm]   Normal displacement of the upper block at the left side
$u_{n(b)}$ [mm]   Normal displacement of the upper block at the right side
$l_{Specimen}$ [mm]   Total length of specimen (= 300 mm)
α [°]   Angle of inclination of the upper block of the specimen

✉ Wengang Dang
dangwg@mail.sysu.edu.cn

1   School of Civil Engineering, Sun Yat-sen University, Zhuhai 519082, China

2   Institute of Geotechnics, TU Bergakademie Freiberg, Gustav-Zeuner-Straße 1, 09599 Freiberg, Germany

1 Introduction

Earthquakes or rock bursts are very complex events, with dynamic excitations in various directions and with variable loads. Stein (1999) reported that an earthquake can alter the shear and normal loads on the surrounding faults. Under certain conditions, cyclic movements along joints/faults under variable normal loads are triggered. Therefore, understanding the cyclic frictional responses of joints under variable normal load conditions is important for the design of rock engineering projects and estimating geological hazards (Liu et al. 2012b, 2013; Liu and Dang 2014; Li et al. 2017; Zhou et al. 2018).

To determine the mechanical responses of joints and rock masses under dynamic load conditions, previous investigations have focused on changes in the normal load on rock joints or rock masses without shearing (Bagde and Petros 2005; Guo et al. 2011; Liu et al. 2011, 2012a; Zhou et al. 2015, 2017; Song et al. 2018) or cyclic shearing under constant normal load conditions (Lee et al. 2001; Ferrero et al. 2010; Mirzaghorbanali et al. 2014; Dang et al. 2017a). Cyclic loading/unloading tests on intact sandstones were performed by Bagde and Petros (2005). They proved that the waveform, amplitude, and frequency of the normal load had significant effects on the fatigue properties. Square waves with a low frequency and amplitude are more likely to damage the samples. Guo et al. (2011) studied the fatigue life and irreversible deformation of salt rock under uniaxial cyclic loading. They found that the fatigue life of salt rock is mainly influenced by its structure as well as the cyclic normal load amplitude. Liu et al. (2011, 2012a) conducted cyclic loading/unloading tests on sandstones and found that the number of cracks increased with increasing impact frequency. Lee et al. (2001) conducted cyclic shear tests on Hwangdeung granite and Yeosan marble. They observed that the peak shear strength and the peak dilation occurred in the first shear cycle. Normal loads and changes of shear directions were the two most important factors affecting the shear strength. Ferrero et al. (2010) conducted cyclic shear tests with f_h ranging from 0.013 to 3.9 Hz and u_{max} ranging from 1.0 to 4.0 mm. The experimental results indicated that the shear displacement amplitude had a significant influence on the peak shear strength. Fathi et al. (2016) investigated the shear mechanism of rock joints under pre-peak cyclic loading conditions. They found that the contact area and the shear strength slightly increased with an increasing number of shear cycles due to contraction. Degradation of the second-order asperities increased with increasing number of shear cycles, while the number of shear cycles had little effect on the residual shear strength.

Direct shear tests have been conducted under variable normal loads (Hobbs and Brady 1985; Olsson 1988; Linker and Dieterich 1992; Hong and Marone 2005; Kilgore et al. 2012, 2017; Molinari and Perfettini 2017; Osei Tutu et al. 2017; Tiwari et al. 2017; Dang et al. 2016a, 2017b, 2018). It is widely accepted that the dynamic normal load weakens the frictional resistance of faults in natural systems (Marone 1998; Rice 2006), and the frictional pattern in response to the step change in normal loads follows a multi-stage process even if the specific results are not exactly the same. Hobbs and Brady (1985) conducted direct shear tests on gabbro under variable normal loads. A large instantaneous change in shear stress was initially observed, which was followed by an exponential time-dependent process. Olsson (1988) performed similar tests on welded tuff, where an immediate steep linear response was initially identified, which was also followed by an exponential time-dependent process. Linker and Dieterich (1992) investigated the frictional response of the stepwise changes of normal loads on Westerly granite using a double direct shear device. A three-stage shear stress changing pattern was observed, with an instantaneous increase, followed by an immediate linear increase with time or shear displacement, finally reaching a steady state (shear stress reached a constant value). Hong and Marone (2005) performed similar tests on quartz gouge. The coefficient of friction changed with sudden changes in the normal load and slip velocity. Kilgore et al. (2012, 2017) studied the frictional response under a stepwise increase in normal loads, stepwise decrease in normal loads, and pulse-like changes of normal loads on a dry bare rock surface of granite, using a double direct shear apparatus. They found that rapid changes in normal loads lead to gradual, nearly exponential changes in shear forces. Changes in the normal load can either strengthen or weaken frictional resistance, depending on joint asperity, slip velocity, and the pattern of normal load. Dang et al. (2016a, 2017b, 2018) performed detailed investigations of the continuous changes of normal load during direct shear tests. The influencing factors of F_s, F_d, f_v, and v were studied in cases where planar joints were made of artificial rock-like material. A time shift between the peak normal load and peak shear force was observed, with a delay in the peak shear force. The minimum coefficient of friction decreased with an increasing amplitude in the normal load oscillation, and increased with increasing shear velocity.

Due to the limitations of the existing shear box devices, there have been few studies on the changes of normal load during cyclic shear. In this paper, we report the results from a wide range of laboratory investigations using our own design of large shear box device (GS-1000), which can apply dynamic loads in the vertical and horizontal directions. The influencing factors F_s, F_d, f_v, f_h, and u_{max} were analysed. Based on the experimental results, a conceptual model was developed for predicting the cyclic shear strength of planar

joints under variable normal loads. In parallel, numerical simulations were conducted on the basis of the laboratory tests. These simulations enabled a better understanding of the cyclic frictional response under cyclic normal load conditions.

2 Laboratory Investigations

2.1 Test Apparatus

Laboratory cyclic shear tests were performed using a large shear box device (GS-1000, Fig. 1a), which is a servo-controlled testing apparatus developed by Konietzky et al. (2012). The GS-1000 shear box consists of vertical and horizontal hydraulic loading systems. The vertical piston provides a constant and superimposed dynamic normal load. The horizontal piston drives the lower shear box, with a cyclic shear rate in the displacement feedback mode. Displacements and forces are measured by linear variable differential transformers (LVDTs), with 1 µm resolution and load cells, with 0.1 kN resolution, respectively. Normal force, shear force, normal displacement, and shear displacement were recorded continuously, with a frequency of 100 Hz. The main technical details of the device are provided in Table 1.
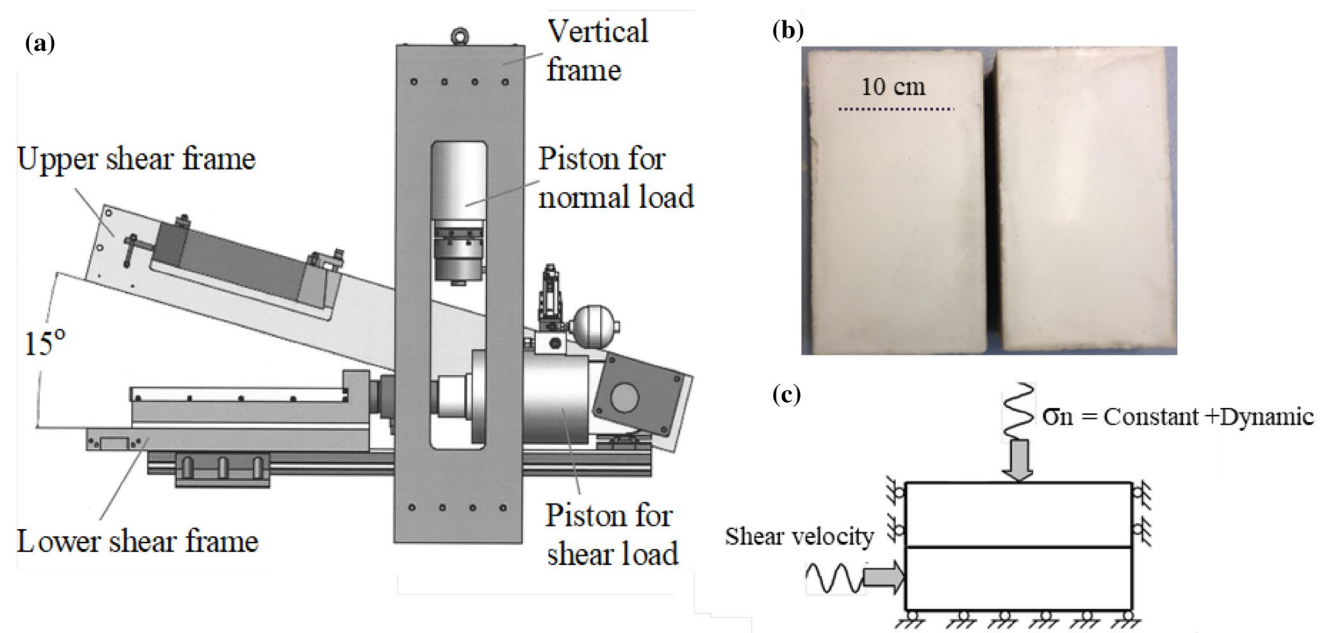
Fig. 1 Testing apparatus and the experimental configuration: **a** main components of the GS-1000 shear box device (Konietzky et al. 2012), **b** artificial rock-like sample with a planar surface, and **c** sketch of the cyclic shear test under a cyclic normal load

Table 1 Main technical data of the device	Item	Value
	Maximum normal load	1000 kN
	Maximum shear load in the forward shear direction	800 kN
	Maximum shear load in the backward shear direction	300 kN
	Maximum shear displacement	50 mm
	Maximum shear velocity	70 mm/s
	Maximum normal impact frequency	40 Hz
	Maximum horizontal shear frequency	40 Hz
	Dynamic load	−500 to +500 kN superimposed on static force level
	Maximum sampling rate	400 Hz (400 data per second)

2.2 Specimen Preparation

A series of artificial rock-like specimens, consisting of CEM I 32.5 R cement (33.3%) and Hohenpockaer glass sand (66.6%), with a block dimension of $30 \times 20 \times 15$ cm (length × width × height) were prepared. As shown in Fig. 1b, the surface was smooth when viewed with the naked eye. The maximum particle size of the components of the specimen was < 1.0 mm (glass sand). The smooth planar joint separated the intact block into two equal halves with a height of 7.5 cm (see Fig. 1b). After 28 days of curing at room temperature (approximately 20 °C), the samples had a uniaxial compressive strength of 19.1 ± 2.4 MPa, a tensile strength of 2.5 ± 0.64 MPa, a Young's modulus of 30 ± 6.4 GPa, and a Poisson's ratio of 0.2 ± 0.03 based on 29 uniaxial compressive tests and 30 Brazilian disc splitting tests.

2.3 Test Procedure

A number of cyclic shear tests under cyclic changes of normal load were conducted as shown in Fig. 1c. Before the cyclic shear tests were conducted, two cycles of normal compression with a loading/unloading rate of 10 kN/min were performed, which re-seated the flat joint and reduced the interspace between the specimen and the shear box. Then the specimen was sheared cyclically under a constant and superimposed dynamic normal load. The dynamic normal load is defined by Eq. 1 and the cyclic shear displacement is defined by Eq. 2

$$F_{sd} = F_d \sin \left(2\pi f_v t \right) \tag{1}$$

$$u_s = u_{max} \sin \left(2\pi f_h t \right). \tag{2}$$

The cyclic shear behaviour was investigated under different F_s, F_d, f_v, f_h and u_{max}. F_s changed from 30 to 360 kN; F_d changed from ± 10 to ± 180 kN; f_v and f_h changed from 0.25 to 5.0 Hz; and u_{max} changed from ± 2.0 to ± 8.0 mm. The detailed input parameters of the cyclic shear tests are documented in Table 2. A total of 57 tests, arranged in 9 groups, were conducted.

3 Test Results and Discussion

In this section, some representative observations of shear forces, normal forces, shear displacements, normal displacements, and k are presented and compared. Additional figures are provided at the end of the paper, which demonstrate the changing pattern of shear force, normal force, and k in each cyclic shear test. In the next chapters, the following definitions are used: forward shear means shear velocity is positive, i.e., the lower specimen moves in the push direction; backward shear means shear velocity is negative, i.e., a lower specimen moves in the pull direction; CCNL means cyclic shear test under constant normal load conditions; DDNL means direct shear test under dynamic normal load conditions.

3.1 Frictional Response

3.1.1 Effects of Constant and Superimposed Normal Loads (CDNL_1)

Figure 2 shows the experimental results for different values of F_s and F_d, but with the same f_h, f_v, and u_{max}. Five cyclic shear tests were conducted: from low F_s (30 kN) and F_d (± 15 kN) to large F_s (360 kN) and F_d (± 180 kN). Shear force and coefficient of friction displayed cyclic variations along with the cyclic variations in normal load and shear direction. Loading led to a contraction of the joint interface and more micro-asperities became interlocked. With increasing static normal load and a superimposed dynamic normal load, the peak shear forces increased, while the peak apparent coefficient of friction k was constant. Under normal loads of 180 ± 90 kN and 360 ± 180 kN (Fig. 2b), the variation in shear forces was different in each shear cycle. The increasing rate of shear force decreased with an increasing number of shear cycles under the normal load conditions described above, which was caused by the progressive damage of the sample under large normal load conditions. As shown in Fig. 2, the apparent coefficient of friction k was followed a square wave curve, with approximately the same peak value. It should be noted that the stable phase of k (i.e., after k reached the peak value) was shorter under a larger normal load. There are two reasons for this: (1) progressive damage of the sample under a large normal load, and (2) increasing shear stiffness of the interface with increasing normal load. Dang et al. (2016b, 2017c) reported that joint stiffness increases with increasing normal load. Therefore, a large shear displacement is needed to reach the peak shear force under a large normal load.

3.1.2 Effects of Amplitudes of Horizontal Shear Displacement (CDNL_2)

To investigate cyclic shear behaviour under the effect of shear displacement amplitude u_{max}, a set of cyclic shear tests similar to CDNL_1 were performed for f_v of 0.5 Hz, f_h of 0.5 Hz, F_s of 90 and 180 kN, F_d of ± 45 and ± 90 kN, and u_{max} of 2, 4, and 8 mm, respectively. Figures 3 and 4 show that the variations in shear force, normal force, and k were similar to CDNL_1. Shear force increased with increasing normal load and k followed a square wave curve, with approximately the same peak value. Under a normal load of

Table 2 Test parameters for cyclic shear tests under DNL conditions

Sample	Stage	F_s (kN)	f_h (Hz)	f_v (Hz)	F_d (kN)	u_{max} (mm)	Cycles$_h$ (–)	Cycles$_v$ (–)
CDNL_1	1	30	0.5	0.5	±15	5	10	10
	2	60	0.5	0.5	±30	5	10	10
	3	90	0.5	0.5	±45	5	10	10
	4	180	0.5	0.5	±90	5	10	10
	5	360	0.5	0.5	±180	5	10	10
CDNL_2	1	90	0.5	0.5	±45	2	10	10
	2	90	0.5	0.5	±45	4	10	10
	3	90	0.5	0.5	±45	8	10	10
	4	180	0.5	0.5	±90	2	10	10
	5	180	0.5	0.5	±90	4	10	10
	6	180	0.5	0.5	±90	8	10	10
CDNL_3	1	90	0.25	1	±45	5	10	40
	2	90	0.5	1	±45	5	10	20
	3	90	1	1	±45	5	10	10
	4	90	2	1	±45	5	20	10
	5	90	3	1	±45	5	30	10
	6	90	4	1	±45	5	40	10
	7	90	5	1	±45	5	50	10
CDNL_4	1	180	0.25	1	±90	5	10	40
	2	180	0.5	1	±90	5	10	20
	3	180	1	1	±90	5	10	10
	4	180	2	1	±90	5	20	10
	5	180	3	1	±90	5	30	10
	6	180	4	1	±90	5	40	10
	7	180	5	1	±90	5	50	10
CDNL_5	1	90	1	0.25	±45	5	40	10
	2	90	1	0.5	±45	5	20	10
	3	90	1	1	±45	5	10	10
	4	90	1	2	±45	5	10	20
	5	90	1	3	±45	5	10	30
	6	90	1	4	±45	5	10	40
	7	90	1	5	±45	5	10	50
CDNL_6	1	180	1	0.25	±90	5	40	10
	2	180	1	0.5	±90	5	20	10
	3	180	1	1	±90	5	10	10
	4	180	1	2	±90	5	10	20
	5	180	1	3	±90	5	10	30
	6	180	1	4	±90	5	10	40
	7	180	1	5	±90	5	10	50
CDNL_7	1	90	0.25	0.25	±45	5	10	10
	2	90	0.5	0.5	±45	5	10	10
	3	90	1	1	±45	5	10	10
	4	90	2	2	±45	5	10	10
	5	90	3	3	±45	5	10	10
	6	90	4	4	±45	5	10	10

Table 2 (continued)

Sample	Stage	F_s (kN)	f_h (Hz)	f_v (Hz)	F_d (kN)	u_{max} (mm)	Cycles$_h$ (–)	Cycles$_v$ (–)
CDNL_8	1	180	0.25	0.25	±90	5	10	10
	2	180	0.5	0.5	±90	5	10	10
	3	180	1	1	±90	5	10	10
	4	180	2	2	±90	5	10	10
	5	180	3	3	±90	5	10	10
	6	180	4	4	±90	5	10	10
CDNL_9	1	90	0.5	0.5	±10	5	10	10
	2	90	0.5	0.5	±20	5	10	10
	3	90	0.5	0.5	±30	5	10	10
	4	90	0.5	0.5	±45	5	10	10
	5	90	0.5	0.5	±60	5	10	10
	6	90	0.5	0.5	±90	5	10	10

90 ± 45 kN, the peak shear force was approximately 95 kN for all shear displacement amplitudes in the forward shear direction, while it was different with different u_{max} in the backward shear direction. For u_{max} of 2, 4, and 8 mm, the absolute values of the peak shear forces were 60, 70, and 80 kN, respectively, which indicates that the absolute value of the peak shear force increased with increasing u_{max} in the backward shear direction. Additionally, the stable phase of k was longer under a larger u_{max} (Fig. 3c). As shown in Fig. 4, the absolute value of the peak shear force increased with increasing u_{max} in the backward shear direction under a normal load of 180 ± 90 kN. Under the same values of f_v, f_h, F_s, and F_d, a smaller u_{max} indicated a smaller shear rate in one shear cycle. At smaller shear rates, a longer time is needed to reach a stable shearing stage (Dang et al. 2018). Therefore, in the forward shearing stage, the shear force was larger under a larger u_{max} than under a smaller u_{max} in the early shearing stage. A longer shearing time in the backward shear direction resulted in a larger reduction of normal load according to Eq. 1. Consequently, the peak shear force reduced with decreasing u_{max} in the backward shear direction.

3.1.3 Effects of Normal Load Impact Frequencies and Cyclic Horizontal Shear Frequencies (CDNL_3 to CDNL_8)

Forty cyclic shear tests, with different values of f_h and f_v, under normal loads of 90 ± 45 kN and 180 ± 90 kN were performed. The shear displacement amplitude was set to 5 mm. As shown in Figs. 5 and 6, the variations in shear force were different compared with CDNL_1 and CDNL_2. The variations in shear force became more complex under different values of f_h and f_v. The following three patterns were identified:

- *When f_h was larger than f_v* The shear force changed cyclically with changing shear direction. The peak shear force in the forward shear direction was almost identical to that in the backward shear direction for all test cases. The peak shear force was observed when the maximum normal load was reached. Variations in the shear force generated square waves, with different amplitudes (Fig. 5a).
- *When f_h was equal to f_v* The peak shear force in the forward shear direction was almost the same in each cycle, and occurred at the point when the maximum normal load was reached. The absolute value of the peak shear force in the backward shear direction was smaller than that in the forward shear direction (only by about 70% of the peak value in the forward shear direction—see Fig. 6c), which was caused by the smaller normal loads in the backward shear direction. For example, at the point of the peak shear force, the maximum normal load was only about 100 kN in the backward shear direction. However, in the forward shear direction, the maximum normal load was 145 kN. The absolute value of the peak shear force decreased with the increasing value of f_h and f_v in the backward shear direction.
- *When f_v was larger than f_h* The variations in the shear force were mainly controlled by the changes in normal load. The peak value of the shear force was similar to the case where $f_h > f_v$ for both the forward and backward shear directions. As shown in Fig. 5d, the variations in the shear force were in phase with the changes in the normal load for a shear displacement ranging from -4 to 4 mm.

Even under complex changes of f_h and f_v, the variations in k were nearly identical to CDNL_1 and CDNL_2, where k followed a square wave curve with the same peak values.
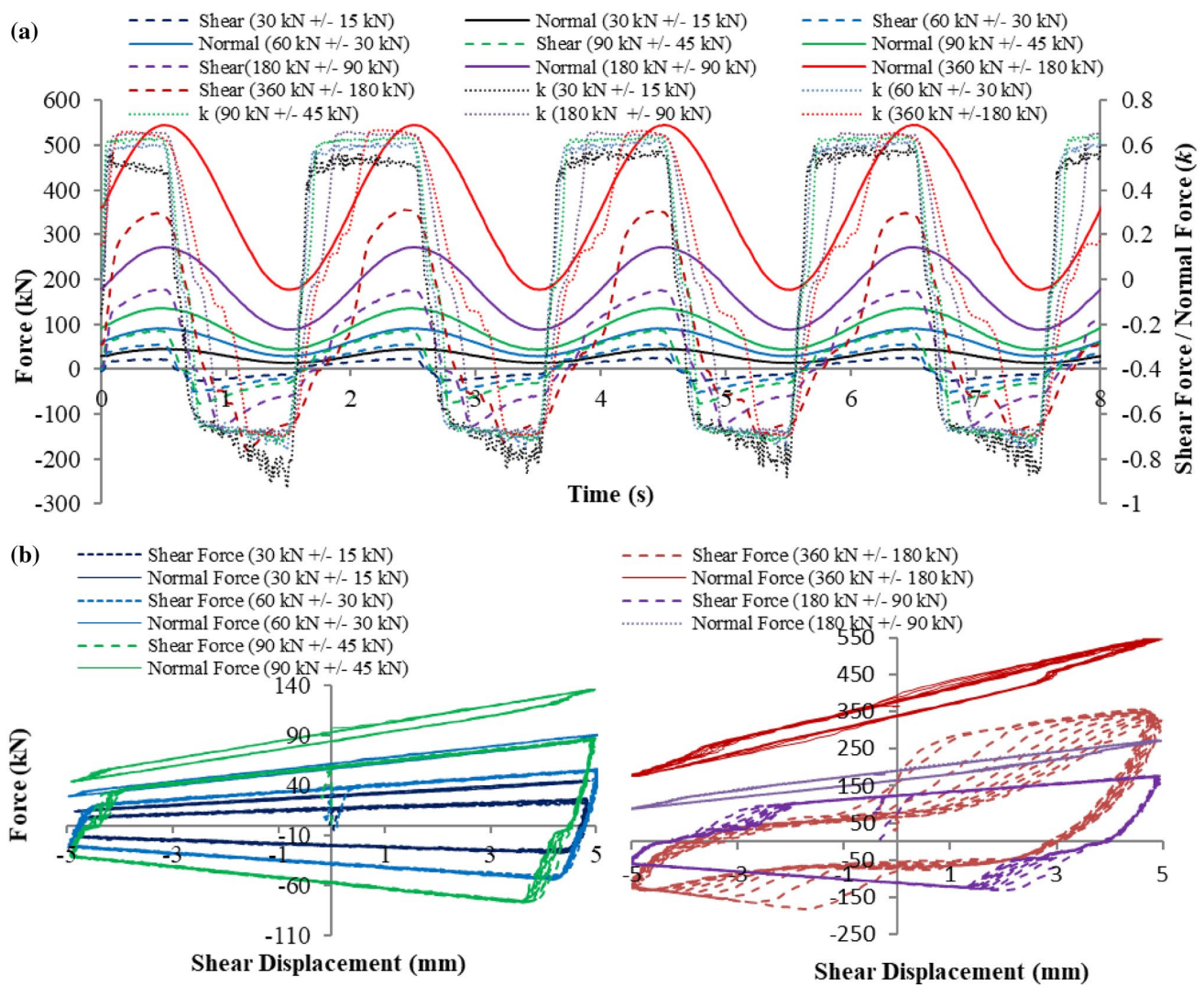
Fig. 2 CDNL_1: experimental results of the cyclic shear test under an f_v of 0.5 Hz, f_h of 0.5 Hz, u_{max} of 5.0 mm, and different F_s and F_d: **a** shear force, normal force, and the ratio between shear force and nor- mal force as a function of time, **b** shear force and normal force as a function of shear displacement

3.1.4 Effects of Normal Impact Force Amplitudes (CDNL_9)

To investigate the effects of impact load amplitude (i.e., F_d) on cyclic shear behaviour, five cyclic shear tests were performed under f_v of 0.5 Hz, f_h of 0.5 Hz, F_s of 90 kN, and F_d of $\pm 10, \pm 20, \pm 30, \pm 45$, and ± 60 kN, respectively. The variations in shear force, normal force, and k are shown in Fig. 7. It was found that the peak shear force increased with increasing F_d in the forward shear direction. However, the peak shear forces in the backward shear direction were constant, and the time in the stable stage (plateau value) decreased with increasing impact load amplitude. Variations in k also generated square wave curves that were nearly identical to each other. This demonstrated that impact load amplitude had little influence on the apparent coefficient of friction k.

3.2 Dilation Response and Damage Pattern

3.2.1 Dilation Response

The cyclic changes of normal displacement were in phase with the cyclic changes of normal load. Taking CDNL_1 for example, in the loading stage, dilation was inhibited, while in the unloading stage, dilation was promoted (Fig. 8a). If the normal displacement at different points of the upper block of the specimen was considered (Fig. 8b), a rotation was observed during each cycle and the inclination angle could be calculated by Eq. 3. The normal displacement went down at one side and went up at the other side of the upper block of the specimen. The corresponding angle of inclination increased until a peak value was reached. Moreover, the inclination angle increased
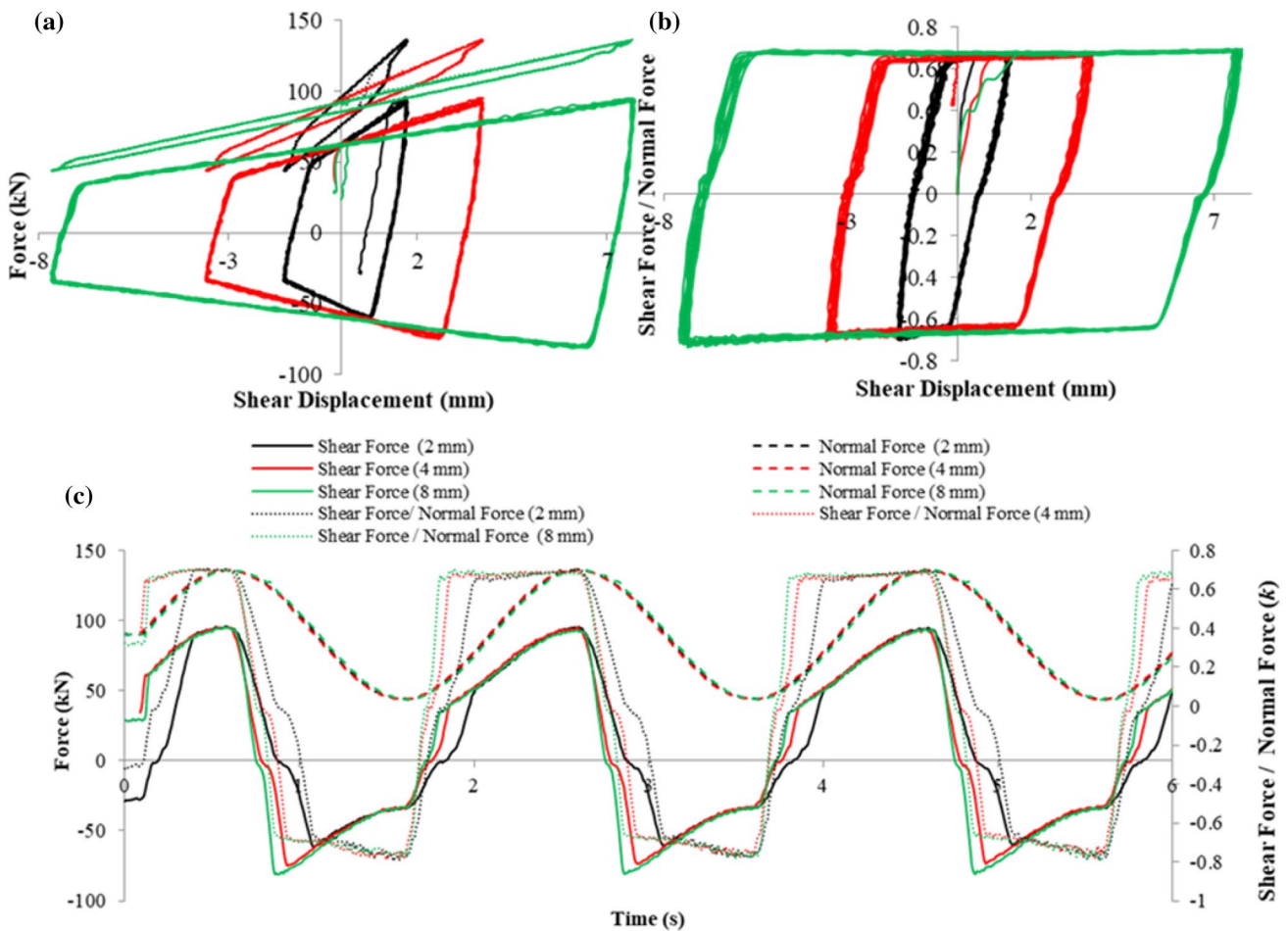
Fig. 3 CDNL_2: experimental results of the cyclic shear test under an f_v of 0.5 Hz, f_h of 0.5 Hz, F_s of 90 kN, F_d of ±45 kN, and u_{max} of 2.0, 4.0 and 8.0 mm, respectively. **a** normal force and shear force as a function of shear displacement, **b** the ratio between shear force and normal force as a function of shear displacement, and **c** shear force, normal force, and the ratio between shear force and normal force as a function of time
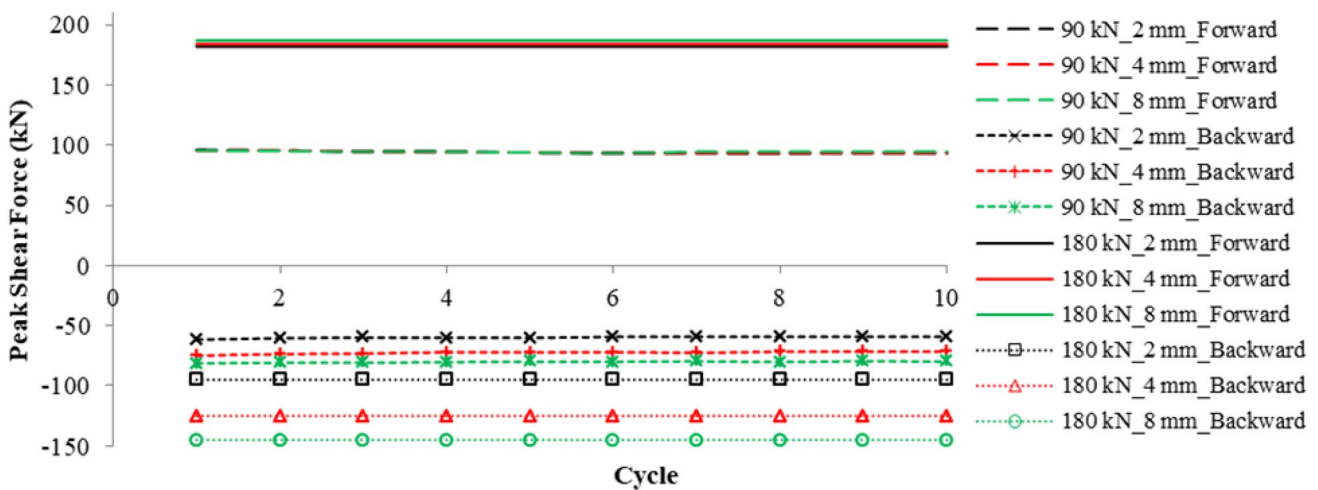
Fig. 4 CDNL_2: peak shear force as a function of the number of shear cycles under an f_v of 0.5 Hz, f_h of 0.5 Hz, F_s of 90 and 180 kN, F_d of ±45 and ±90 kN, and shear displacement amplitude u_{max} of 2, 4, and 8 mm, respectively
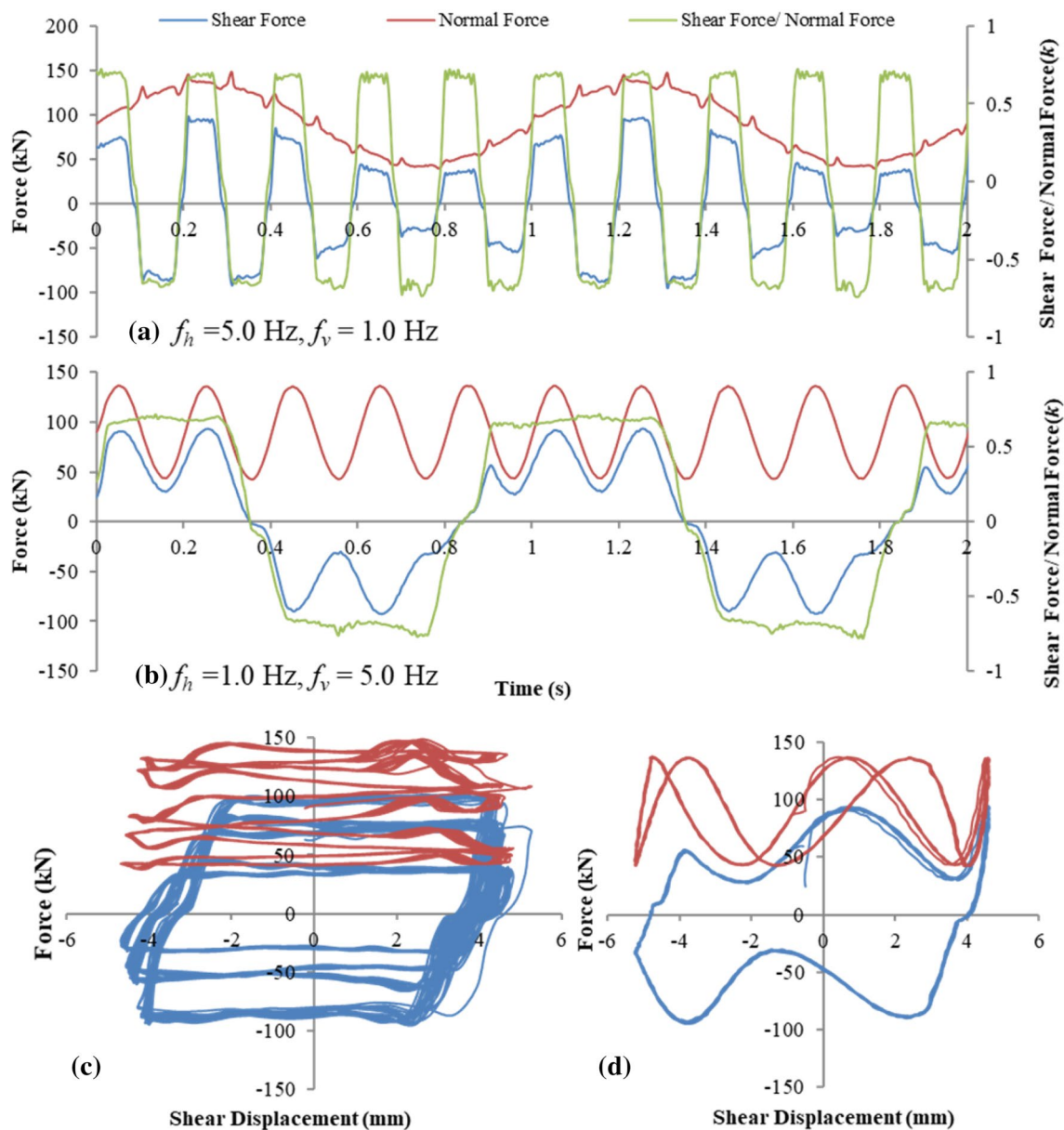
Fig. 5 Shear force, normal force, and the ratio between shear force and normal force as a function of time and shear displacement under an F_s of 90 kN, F_d of ± 45 kN, u_{max} of 5.0 mm: **a** and **c** f_v of 1.0 Hz and f_h of 5.0 Hz, **b** and **d** f_v of 5.0 Hz and f_h of 1.0 Hz

with increasing normal load. The number of shear cycles had a significant effect on the normal displacement but had little effect on the angle of inclination. Figures 8c–f show that normal displacement (settlement) increased with an increasing number of shear cycles, which was mainly caused by the fatigue of the sample under the cyclic normal load (Song et al. 2018). Moreover, the settlement also increased with increasing normal load level.

$$\alpha = \arctan\left(\frac{\left|u_{n(a)}\right| + \left|u_{n(b)}\right|}{l_{Specimen}}\right) \tag{3}$$

3.2.2 Damage Pattern

Figure 9 shows a typical damage pattern of the samples after the cyclic shear test. The damaged area was mainly located at the two edges of the joint surface. Furthermore, a large quasi-static normal load and large superimposed dynamic normal load resulted in serious damage to the sample.

3.3 Comparison with the CCNL and DDNL Tests

A series of CCNL and DDNL tests were performed using the same material and testing device as in our previous studies
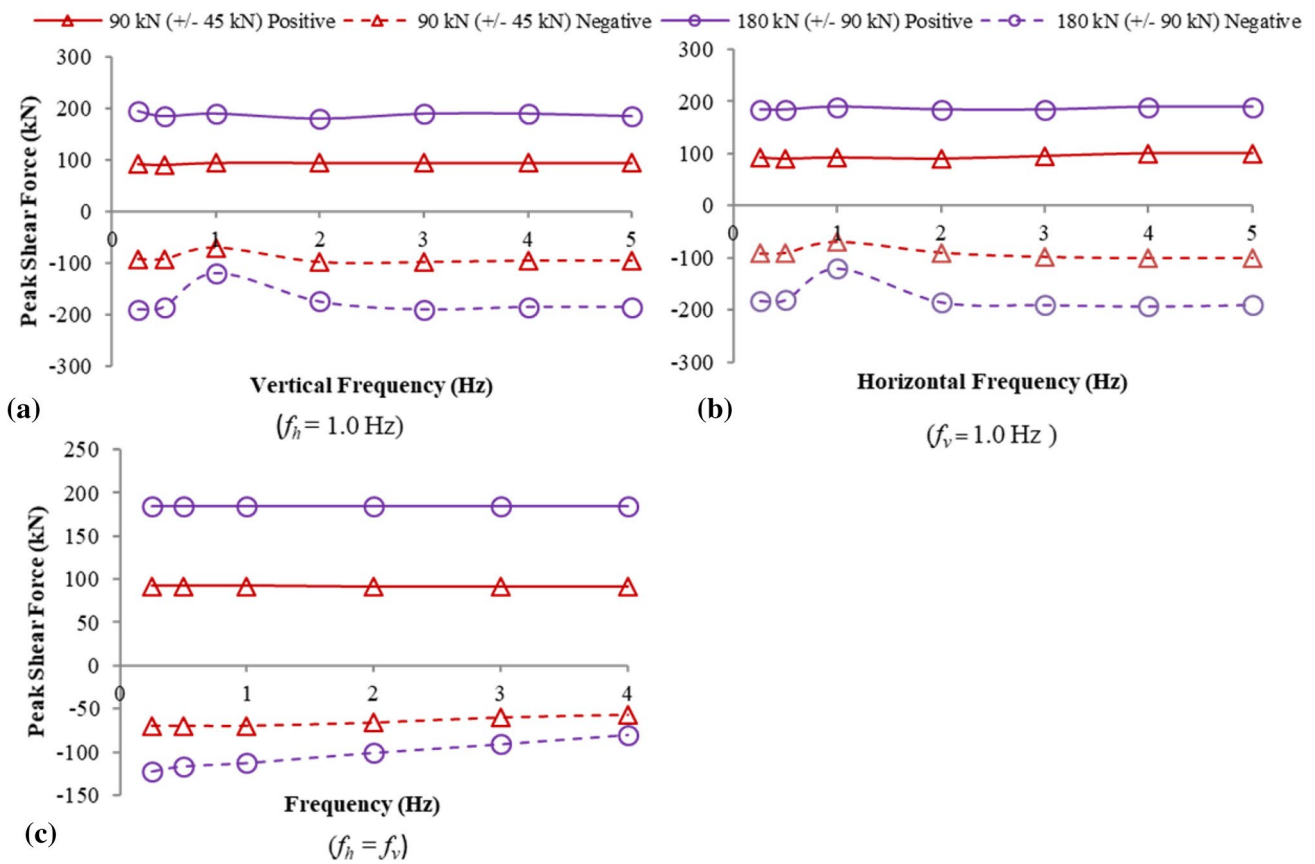
Fig. 6 CDNL_3 to CDNL_8: experimental results of the peak shear forces under an F_s of 90 and 180 kN, F_d of ± 45 and, ± 90 kN, and u_{max} of 5.0 mm: **a** f_h of 1.0 Hz, different values of f_v, **b** f_v of 1.0 Hz, different values of f_h, and **c** $f_h = f_v$
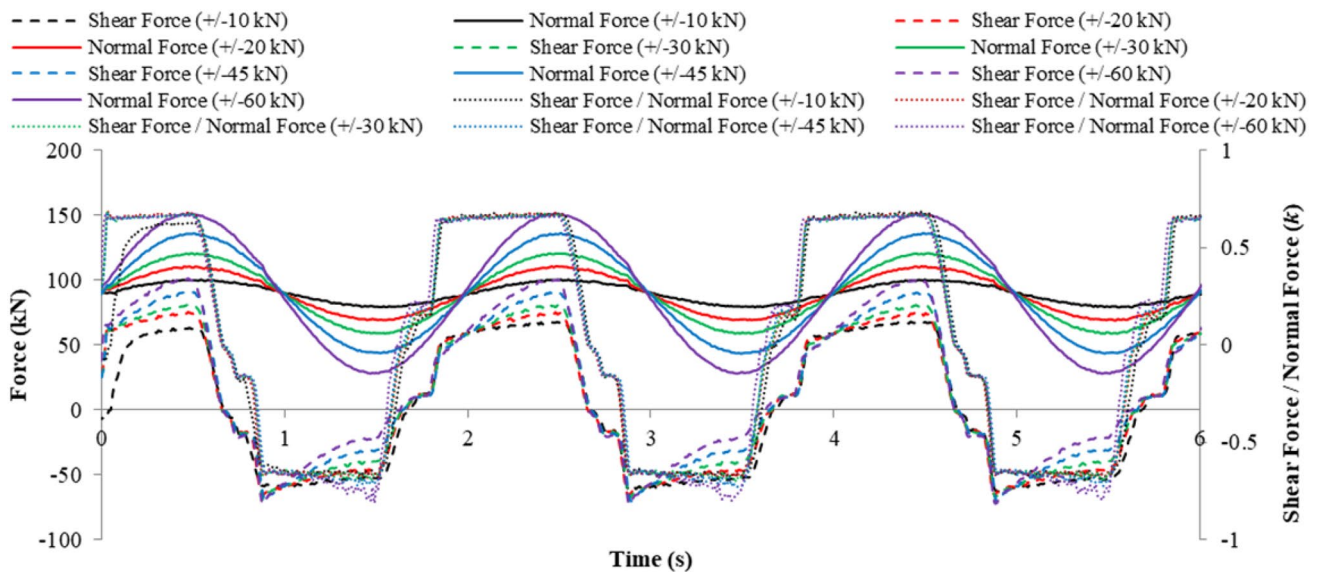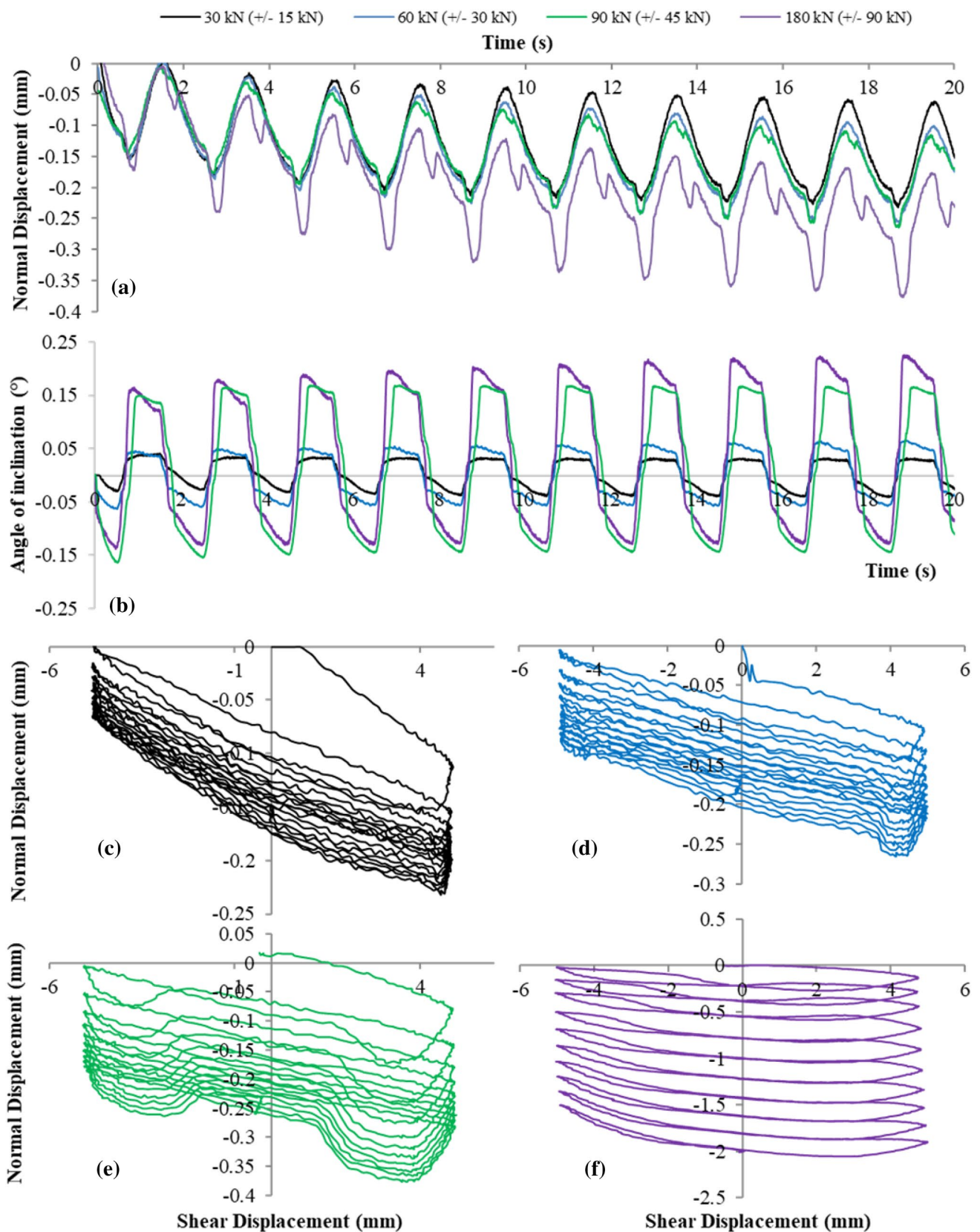

Fig. 7 CDNL_9: experimental results for the shear force, normal force, and the ratio between shear force and normal force as a function of time and shear displacement under an f_v of 0.5 Hz, f_h of 0.5 Hz, F_s of 90 kN, u_{max} of 5.0 mm, and F_d of $\pm 10, \pm 20, \pm 30, \pm 45$, and ± 60 kN, respectively

Fig. 8 CDNL_1: experimental results of the cyclic shear test under an f_v of 0.5 Hz, f_h of 0.5 Hz, u_{max} of 5.0 mm, and different F_s and F_d: **a** normal displacement as a function of time, **b** angle of inclination as a function of time, **c–f** normal displacement as a function of shear displacement under a normal load of 30 ± 15 kN, 60 ± 30 kN, 90 ± 45 kN and 180 ± 90 kN, respectively

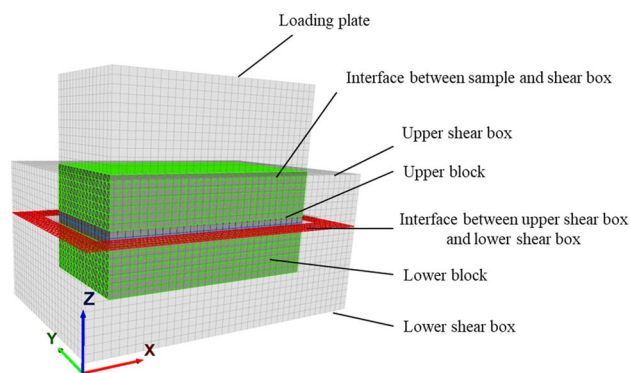Fig. 9 Typical damage pattern of the sample after the shear test

Fig. 10 General model setup used for simulating the cyclic shear test with Fast Lagrangian Analysis of Continua in Three-Dimensions (FLAC[3D]) software

(Dang et al. 2017c, 2018). The general changing pattern of k in this study was similar to that in CCNL tests, during which k also displayed cyclic variations along with cyclic variations in shear direction, and k was nearly constant at the stable shearing stage (Dang et al. 2017c). However, the changing pattern of k was very different compared with the DDNL tests (Dang et al. 2018). The apparent coefficient of friction k displayed cyclic variations along with the cyclic variations in normal load when the shear process reached the stable stage. But in this study, k was nearly constant even with the cyclic variations in normal load at the stable stage (see Fig. 5a and b), which indicated that changes in shear direction met changes in normal load generating a distinct changing pattern of k. Dang et al. (2018) reported that changes in shear velocity encounters changes in normal forces leading to a special changing pattern of k. Because the shear velocity was controlled by Eq. 2 during cyclic shearing, the shear velocity changed along with the changes in shear displacement. The special changing pattern of k might be caused by the changes in shear velocity encountering changes

of normal load. The physical reason of this behaviour needs further investigation.

4 Numerical Simulation

4.1 Setup of the Numerical Model

The numerical code FLAC[3D] was used to simulate the cyclic frictional behaviour of the planar joints under a cyclic normal load. The numerical model consisted of five parts (see Fig. 10): the loading plate, upper shear box, upper block of the specimen, lower shear box, and lower block of the specimen. Interface elements were defined between the loading plate and upper block of the specimen; upper shear box and upper block of the specimen; upper shear box and lower shear box; upper block of the specimen and lower block of the specimen; and lower shear box and lower block of the specimen. The size of the specimen considered in the numerical model was identical to that used in the laboratory test. The numerical model consisted of 34,403 grid points, 27,600 zones, 3417 interface nodes, and 6312 interface elements. The upper shear box was fixed in the X and Y directions, and the lower shear box was fixed in the Y and Z directions. In the simulation process, a constant normal load was applied to the loading plate. When the whole model had reached equilibrium, a cyclic normal load controlled by Eq. 1 was applied at the loading plate. At

Table 3 Parameters of the interface

ID	Kn/[Pa/m]	Ks/[Pa/m]	Friction/[°]	Cohesion/[MPa]	Tension/[MPa]	Dilation/[°]	Position
1	3.0e10	3.0e10	15	0	0	0	Between testing sample and shear box
2	6.0e10	6.0e10	15	0	0	0	Between bottom shear box and top shear box
3	(0.4–6.2)e10	(0.4–6.2)e10	39.5	0	0	0	Between bottom specimen and top specimen

Fig. 11 Displacement vectors, normal force, shear force, angle of inclination, and shear displacement as a function of time under an F_s of 90 kN, F_d of ± 45 kN, u_{max} of 5.0 mm: **a** f_v of 1.0 Hz and f_h of 1.0 Hz, **b** f_v of 1.0 Hz and f_h of 5.0 Hz, **c** f_v of 5.0 Hz and f_h of 1.0 Hz
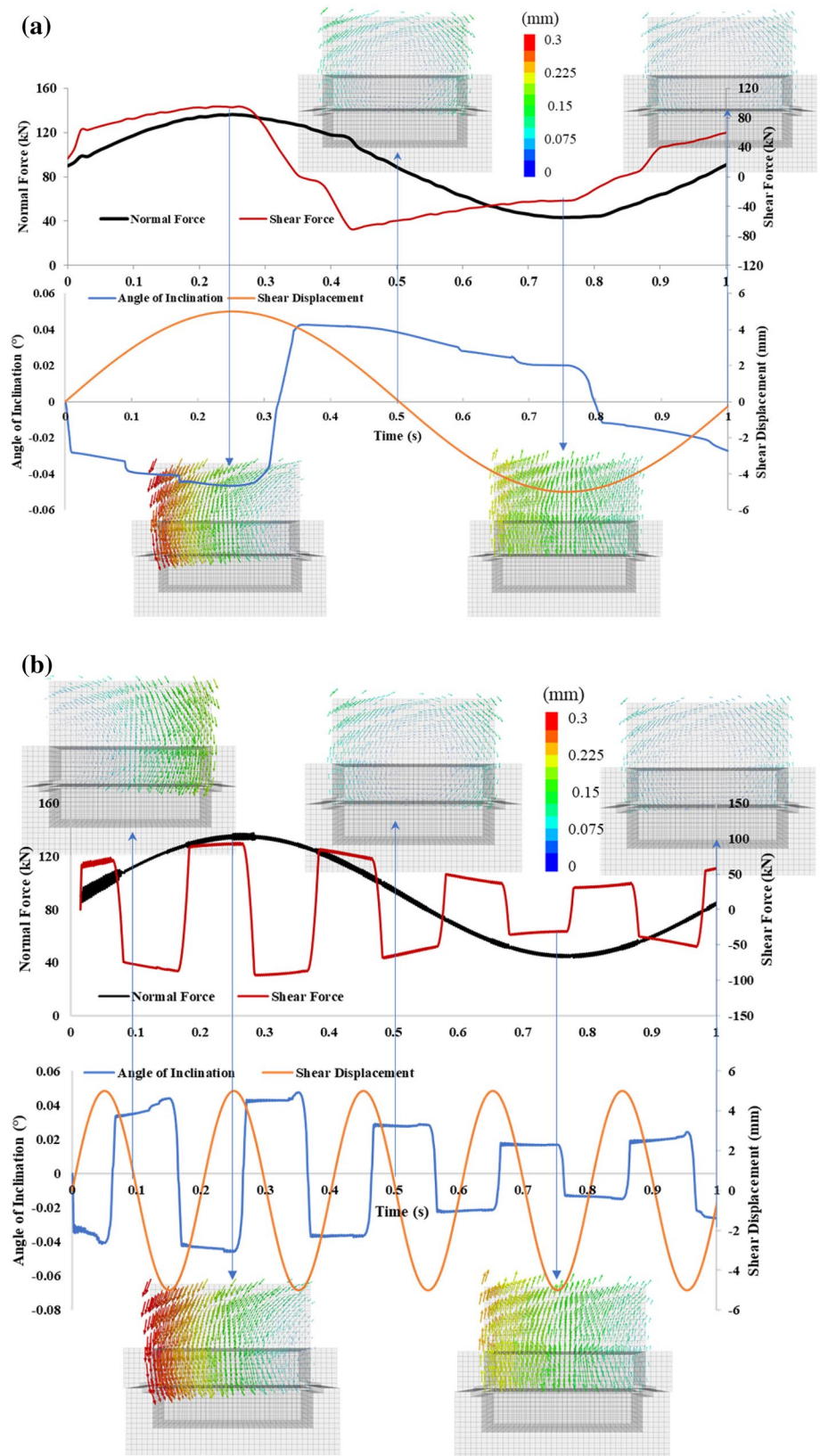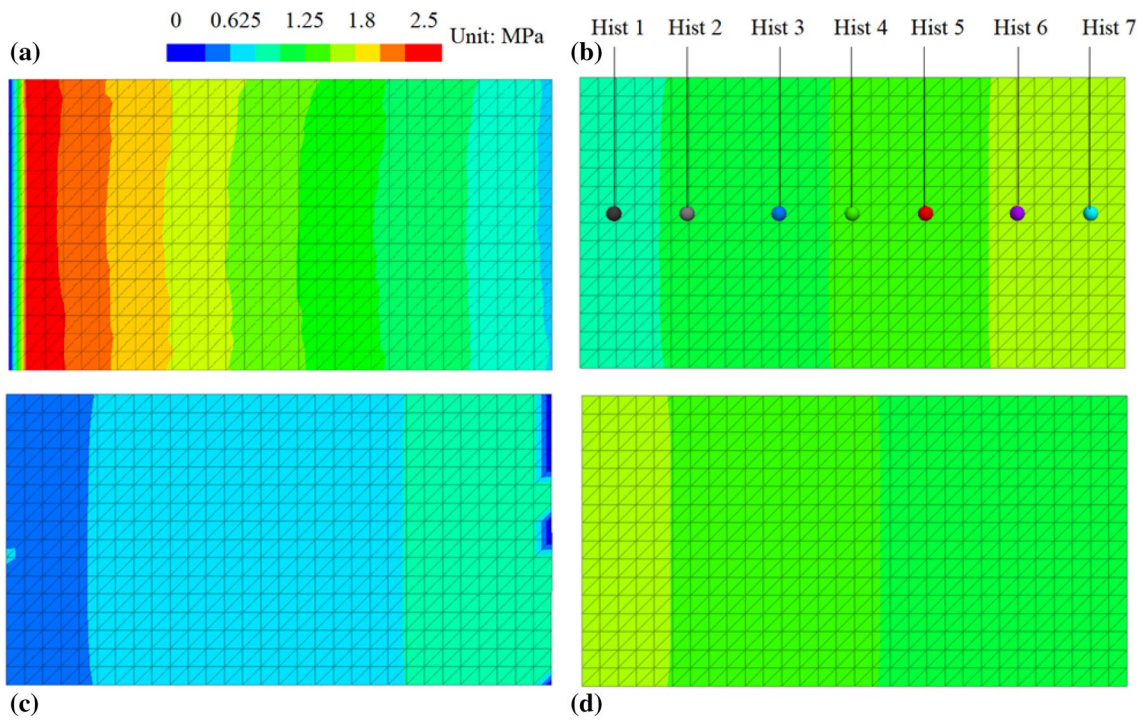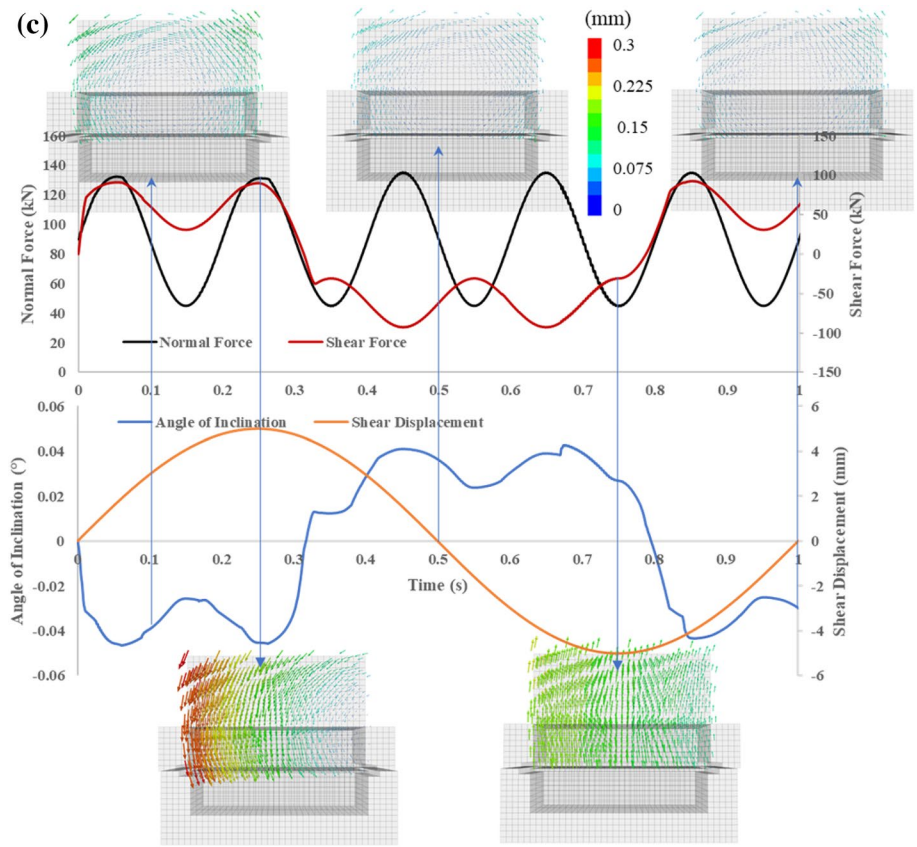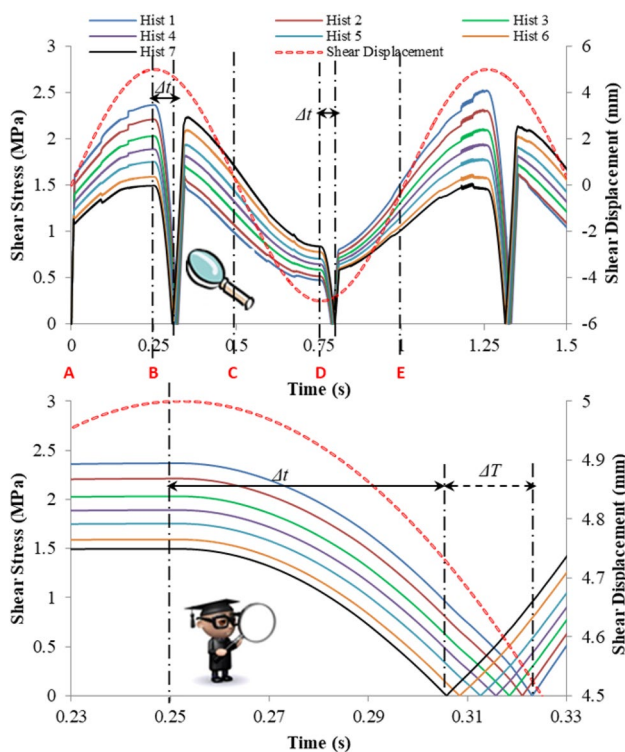
Fig. 11 (continued)

Fig. 12 Interface normal stress under an F_s of 90 kN, F_d of ± 45 kN, u_{max} of 5.0 mm, f_v of 1.0 Hz, and f_h of 1.0 Hz at different shear cycles: **a** 0.25 cycles, **b** 0.5 cycles, **c** 0.75 cycles, and **d** 1 cycle

Fig. 13 Shear stress at the interface as a function of time under an F_s of 90 kN, F_d of ± 45 kN, u_{max} of 5.0 mm, f_v of 1.0 Hz, and f_h of 1.0 Hz

the same time, a cyclic shear velocity controlled by Eq. 2 was applied at the lower shear box. The mechanical parameters of the interfaces are shown in Table 3 and the mechanical parameters of the specimen are shown in Sect. 2.2. Young's modulus and Poisson's ratio of the shear box were 200 GPa and 0.3, respectively. The elastic constitutive model was used for the calculation of the loading plate, upper shear box, and lower shear box. Mohr–Coulomb constitutive models were used for the calculation of the specimen and interfaces. In the calculation process, several useful data were recorded, which reflected the changes in normal stress and shear stress of the interface between the upper and lower blocks of the specimen.

4.2 Numerical Simulation Results

4.2.1 Movement of the Upper Block of the Specimen and the Loading Plate

Figure 11 shows the typical movement pattern of loading plate and upper block of the specimen, indicating a rotational pattern during cyclic shearing. The rotation was caused by uneven force distribution and the rotational patterns were governed by changes in the normal load and shear direction. As with the laboratory tests, the cyclic changes of normal displacement were in phase with the cyclic changes of normal load. The shear displacement amplitude, u_{max}, and impact normal load amplitude (i.e., F_d) only affected the scale of the rotation, with little effect on the rotation orientation. Only the frequency (i.e., f_v and f_h) effects are presented here.

As demonstrated in Fig. 11a, when f_v was equal to f_h, i.e., from 0 to 0.25 s, as controlled by the cyclic shear load, the lower shear box and the lower block of the specimen moved in the forward direction, finally reaching the maximum displacement. The normal load increased with ongoing shear displacement. The peak normal load coincided with the point of the maximum shear displacement in the forward shear direction. An inclination at the left side of the loading plate and the upper block of the specimen was observed. The inclination angle reached its peak value at the point of the maximum shear displacement. From 0.25 to 0.75 s, the shear direction was reversed, and the lower shear box and the lower block of the specimen moved in the backward shear direction. Simultaneously, the normal load started to decrease with ongoing shear displacement. Due to the reversal of shear direction and unloading of the normal load, the left side inclination of loading plate and upper block of the specimen diminished step by step. Eventually, the left side inclination became inclined to the right side, i.e., a clockwise rotation. From 0.75 to 1.0 s, the shear direction reversed again. At the same time, the normal load started to increase with increasing shear displacement and the normal load and shear displacement reached the initial value at 1.0 s, i.e., both the superimposed cyclic load and the shear displacement were zero. The right side inclination of the loading plate and upper block of the specimen gradually diminished. Eventually, the right side inclination turned into a left side inclination, i.e., an anti-clockwise rotation.

The movement patterns of the upper block of the specimen became more complicated when f_v was not equal to f_h. As shown in Fig. 11b, when f_h was larger than f_v, the rotation orientation changed cyclically with a change in shear direction. From 0 to 0.25 s, as controlled by Eq. 1, the normal load gradually increased. The plateau level of the inclination angle increased with the ongoing number of cyclic shear cycles. From 0.25 to 0.75 s, the normal load steadily decreased. The plateau level of the inclination angle decreased with ongoing number of cyclic shear cycles. This indicates that the inclination angle increased with an increase in normal load. As shown in Fig. 11c, when f_v was larger than f_h, the absolute value of the inclination angle was also in phase with the normal force, which increased with an increase in normal load. The cyclic changes in the normal load resulted in fluctuations in the plateau level of the inclination angle.
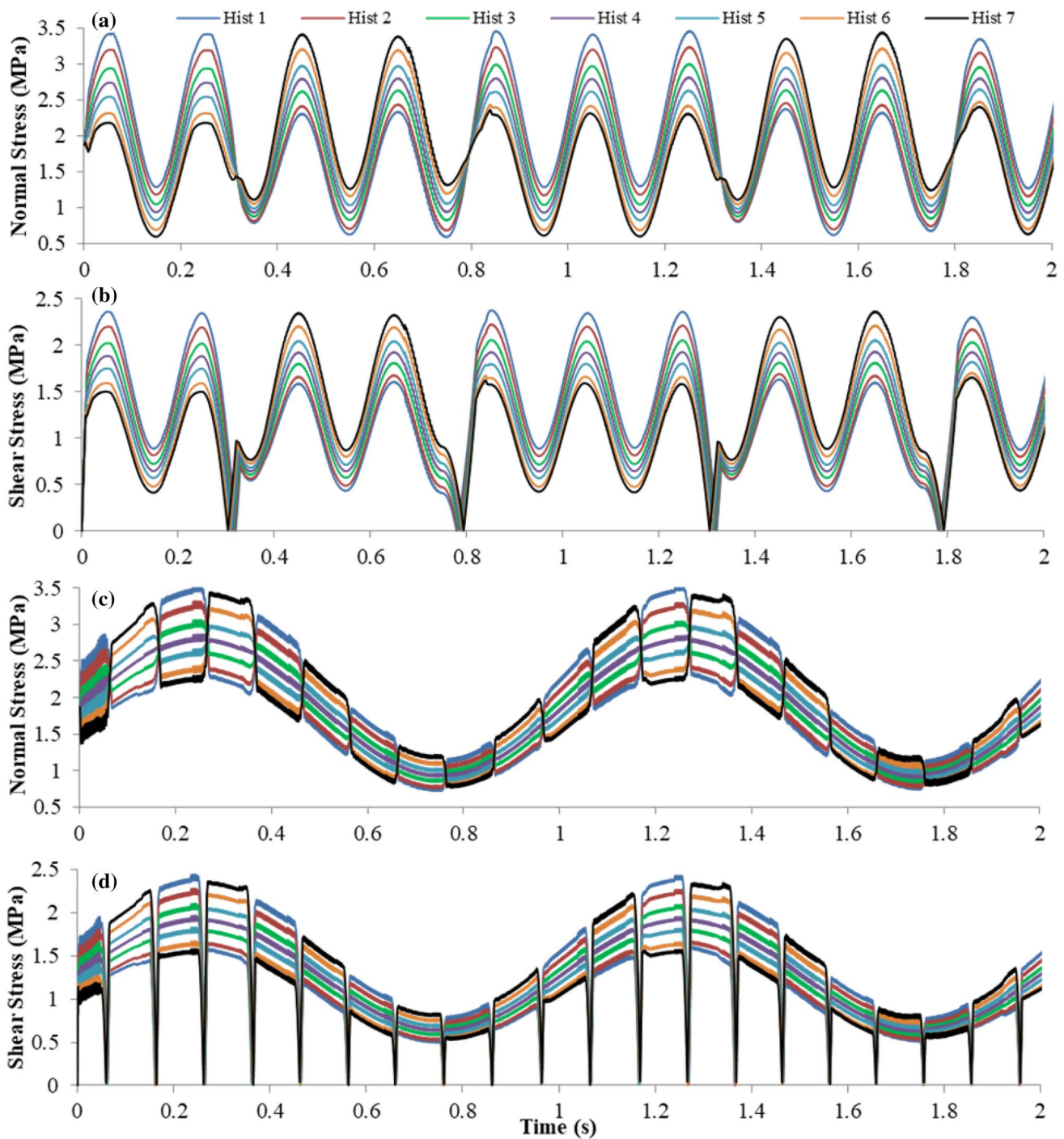
Fig. 14 Normal stress and shear stress at the interface as a function of time under an F_s of 90 kN, F_d of ± 45 kN, and u_{max} of 5.0 mm with different f_v and f_h: **a** and **b** f_v of 5.0 Hz and f_h of 1.0 Hz, **c** and **d** f_v of 1.0 Hz and f_h of 5.0 Hz

4.2.2 Stress Distribution Pattern at the Interface

Due to the inclination of the upper block of the specimen, the stress distributed at the interface became very inhomogeneous (see Figs. 12, 13 and 14), which resulted in a distinct stress gradient along the contact surface. The stress gradient pattern was controlled by the shear displacement and normal load levels. The stress gradient decreased from left to right when the shear displacement occurred in the forward shear direction, and decreased from right to left when the shear displacement occurred in the backward shear direction. In addition, the inhomogeneous stress deviation (i.e.,
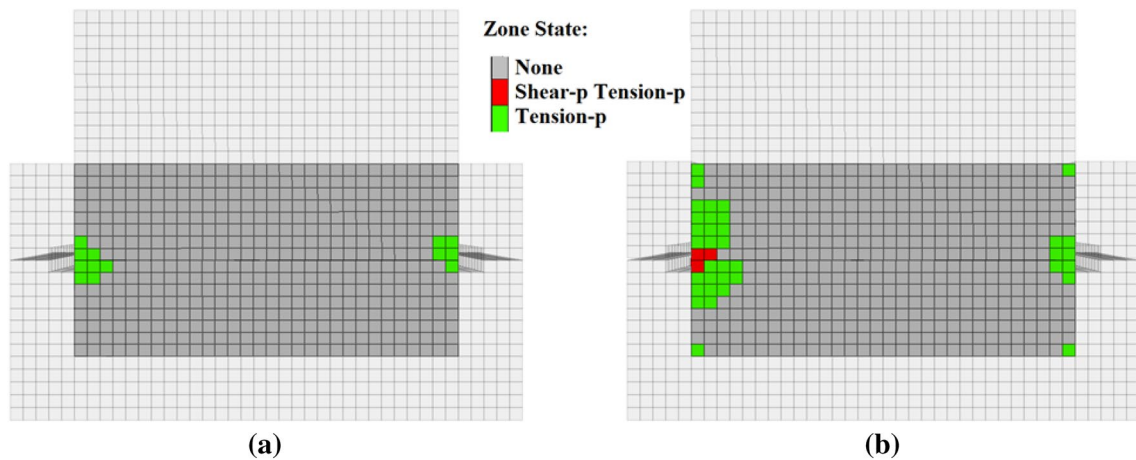
Fig. 15 Zone plasticity state under an F_s of 90 kN, F_d of ± 45 kN, u_{max} of 5.0 mm, f_v of 1.0 Hz, and f_h of 1.0 Hz: **a** 1.0 cycle, **b** 10.0 cycles
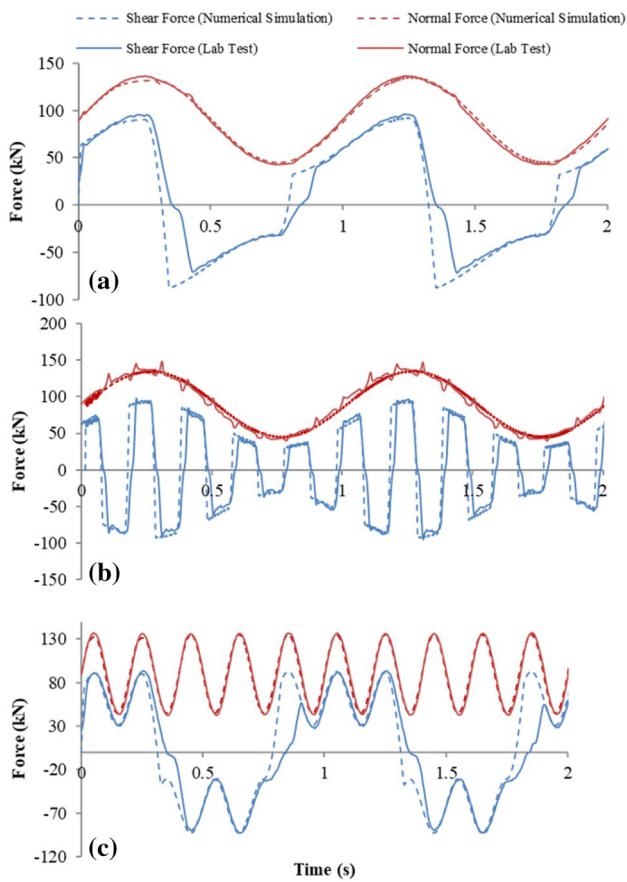

Fig. 16 Comparison between the laboratory test results and numerical simulation results: **a** f_v of 1.0 Hz and f_h of 1.0 Hz, **b** f_v of 1.0 Hz and f_h of 5.0 Hz, **c** and **d** f_v of 5.0 Hz and f_h of 1.0 Hz
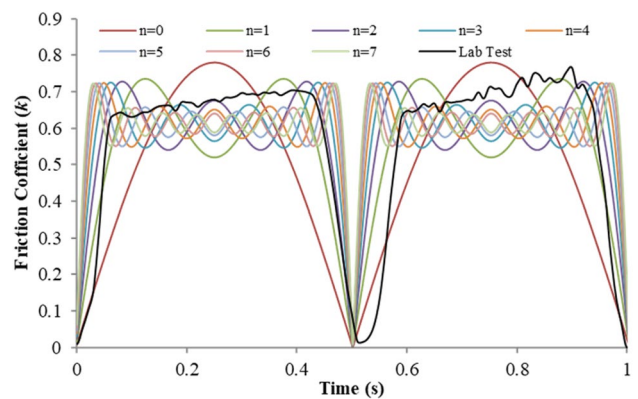

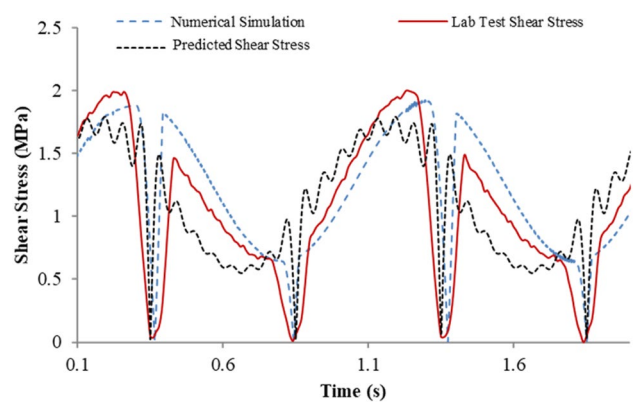**Fig. 17** Synthesized apparent coefficient of friction (k) as a function of time

Fig. 18 Comparison between the numerical simulation of the shear stress, laboratory test shear stress, and predicted shear stress under an F_s of 90 kN, F_d of ± 45 kN, u_{max} of 5.0 mm, f_v of 1.0 Hz, and f_h of 1.0 Hz

the scale of the stress gradient) along the interface increased with increasing normal load and increasing shear displacement. Changes in the shear direction altered the interface

stress gradient orientation and the maximum stress was concentrated at the two edges of the interface regardless of changes in the normal load or shear direction. The inhomogeneous stress at the interface was caused by the unbalanced force distribution inside the sample during shearing, with a detailed explanation reported previously (Dang et al. 2016b).

It should also be noted that there was a time shift in the reversal points between the shear displacement and interface shear stress, i.e., the interface stress reversal happened shortly after the reversal of shear direction (see Fig. 13), which was mainly caused by the shear stiffness of the interface. Furthermore, the reversal points of the normal and shear stress along the interface also followed the time sequence.

4.3 Comparison Between the Simulated and Measured Data

High stresses were concentrated locally at the two edges of the interface, which resulted in damage at the two edges of the specimen (see Fig. 15). The damage accumulated as the number of cyclic shear cycles increased. The simulated damage of the specimen agreed well with the experimental results, as shown in Fig. 9. Test data from three tests (as shown in Fig. 16) were selected to calibrate the numerical model. It was found that laboratory test results and numerical simulations showed a good agreement, which proved that the proposed numerical model was capable of reproducing the mechanical behaviour of planar joints under cyclic normal load conditions during cyclic shearing.

5 Shear Strength Prediction

As explained in Sect. 3 and the appendix, the variations in k followed a square wave curve, with nearly identical peak values in all the laboratory tests. The period of k was in agreement with the changes in f_h. Square wave curves can be synthesized by sinusoidal waves by applying a Fourier transformation (Bochner and Chandrasekharan 1949). Therefore, k can be described by Eq. 4, in which a larger n generates a better approximation of the square wave curve of k (shown in Fig. 17). The apparent normal load can be obtained by summing the constant normal load and the superimposed cyclic normal load. The apparent normal stress can be described by Eq. 5. An expression for predicting cyclic shear strength under cyclic normal load conditions is given by Eq. 6.

$$f(t) = \text{ABS} \left(K \sum_{n=0}^{n_{\max}} \left(\frac{1}{2n+1} \sin\left((2n+1)t\right) \right) \right)$$
$$\ldots (n \in (0, 1, 2, 3, \ldots)) \tag{4}$$

$$\sigma_n = \frac{F_s + F_d \sin(2\pi ft)}{S} \tag{5}$$

$$\tau = f(t)\sigma_n = \text{ABS} \left(K \sum_{n=0}^{n_{\max}} \left(\frac{1}{2n+1} \sin\left((2n+1)t\right) \right) \right)$$
$$\cdot \frac{F_s + F_d \sin(2\pi ft)}{S} \ldots (n \in (0, 1, 2, 3, \ldots)). \tag{6}$$

Figure 18 shows a comparison between the numerically simulated shear strength, analytically predicted shear strength, and experimentally obtained shear strength. The experimental shear strength result was in close agreement with the numerical and analytical values. This indicates that the derived expression could predict the cyclic shear strength of the planar joints under cyclic normal load conditions. It should be noted that due to the limited number of tests, limited specimen material, and tiny joint roughness, Eq. 6 is a preliminary equation at this stage. The confirmation of the proposed mathematical equation needs further investigation, with attention given to the fatigue phenomenon of the material.

6 Conclusions

The cyclic frictional behaviour of planar joints under cyclic normal load conditions was investigated through laboratory tests and numerical simulations. The main findings of the research are the following:

- The apparent coefficient of friction k changes cyclically with changes in shear direction, where k follows a square wave curve with nearly identical peak values.
- The variations in k are only slightly influenced by changes in F_s, F_d, f_v, f_h, and $u_{\max}$.
- There is a clockwise or anti-clockwise rotation of the upper block of the specimen during cyclic shearing.
- Numerical simulations document the inhomogeneous stress distribution along the interface during cyclic shearing. Maximum and minimum stresses are located at the two edges of the interface.
- The numerical simulations also proved a distinct time shift in the reversal points between the shear displacement and interface shear stress. The reversal points of the shear stress along the interface follow the time sequence.
- A mathematical equation that is proposed could be the baseline for the development of a further shear strength criterion.

In this study, the roughness of the surface and the lifetime of the specimen due to cyclic fatigue (e.g., Song et al. 2018), which could significantly influence the frictional behaviour of joints, were not taken into account. Moreover, water pressure variation (e.g., Dang et al. 2019) during cyclic shear is

often encountered in nature. Further investigations focusing on the cyclic frictional behaviour influenced by joint asperities and water pressure variations are required.

Appendix

See Fig. 19.

CDNL_1-1

CDNL_1-2

CDNL_1-3

CDNL_1-4

CDNL_1-5
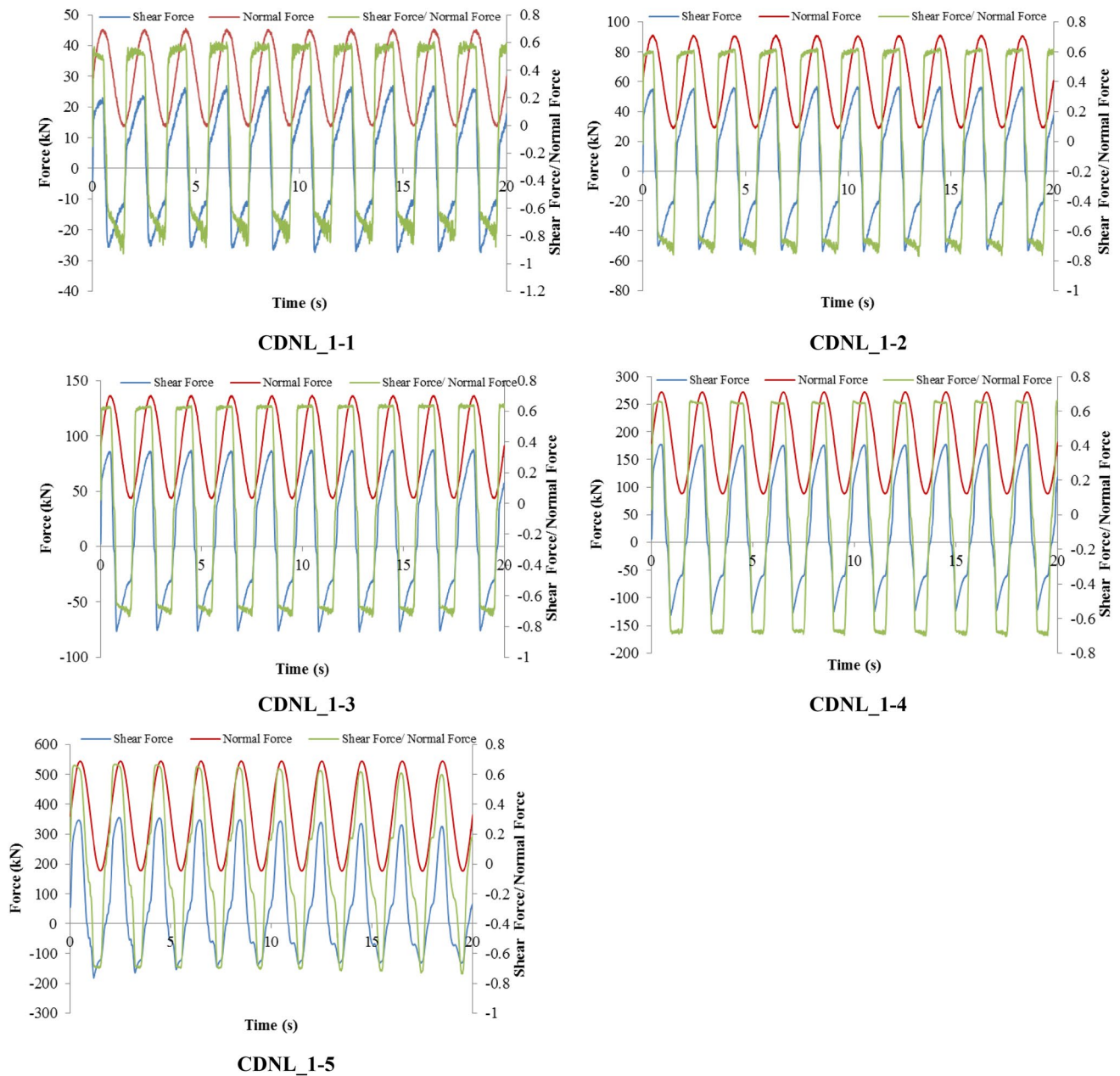
Fig. 19 Shear force, normal force and shear force/normal force vs. time
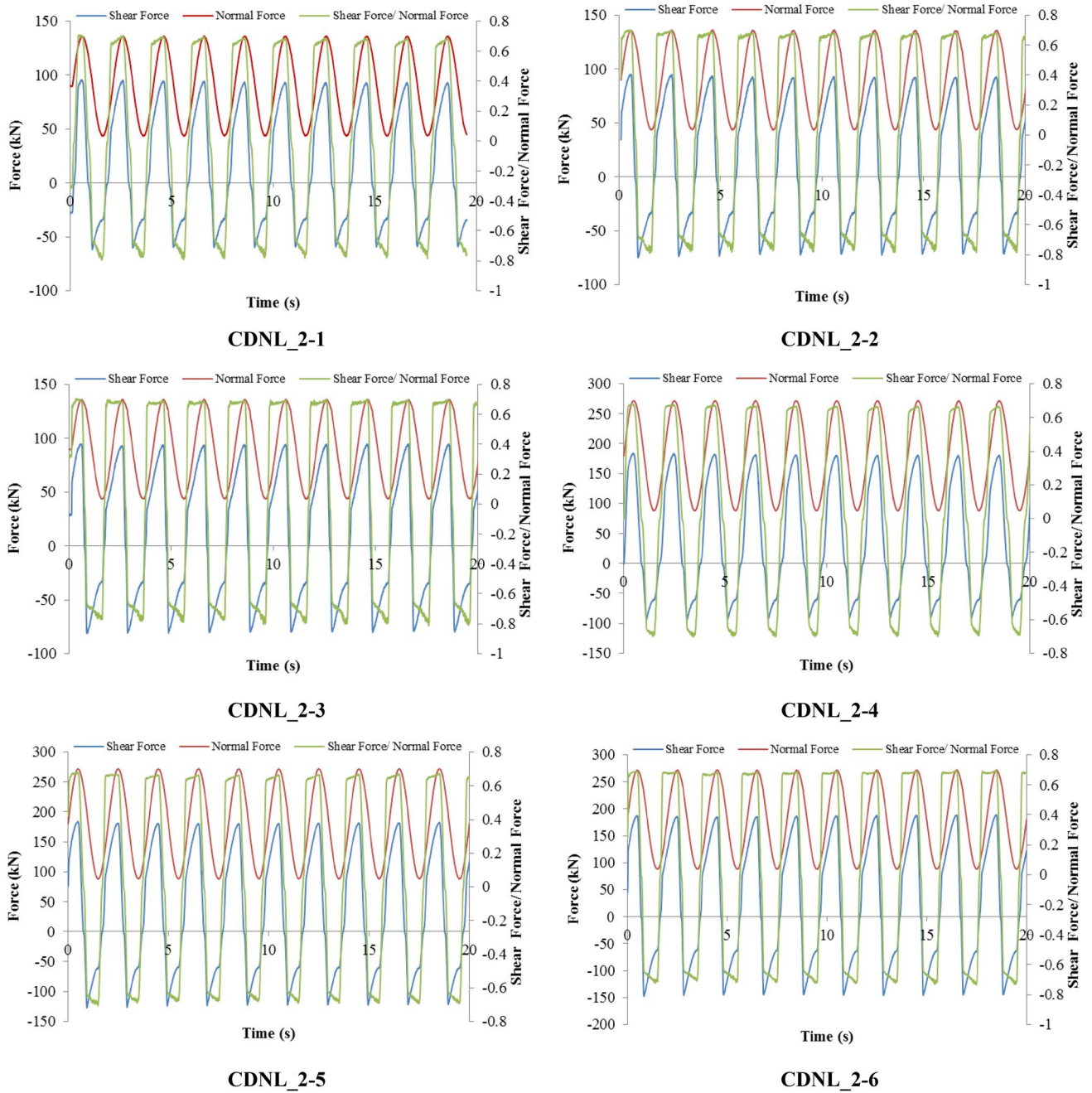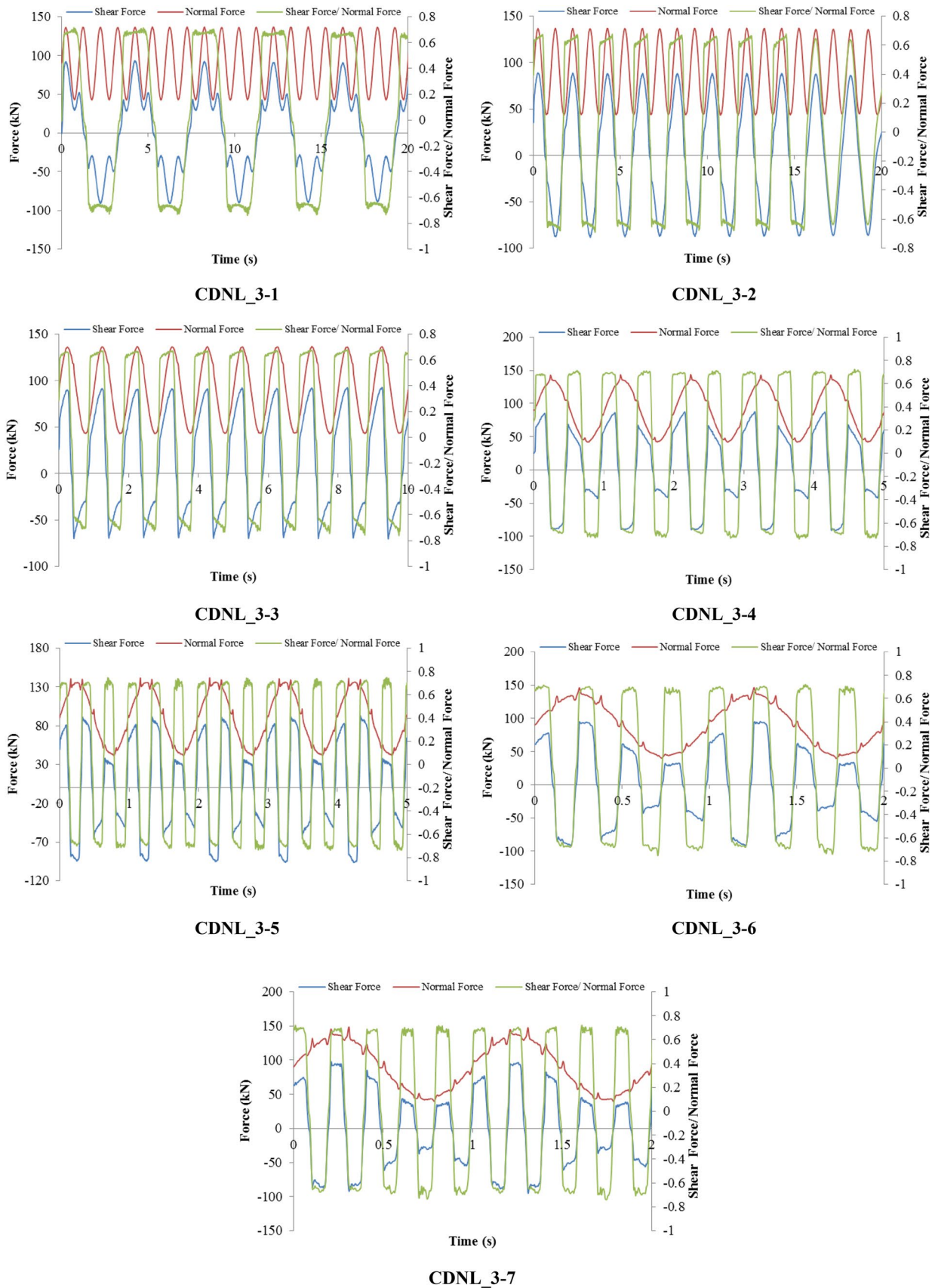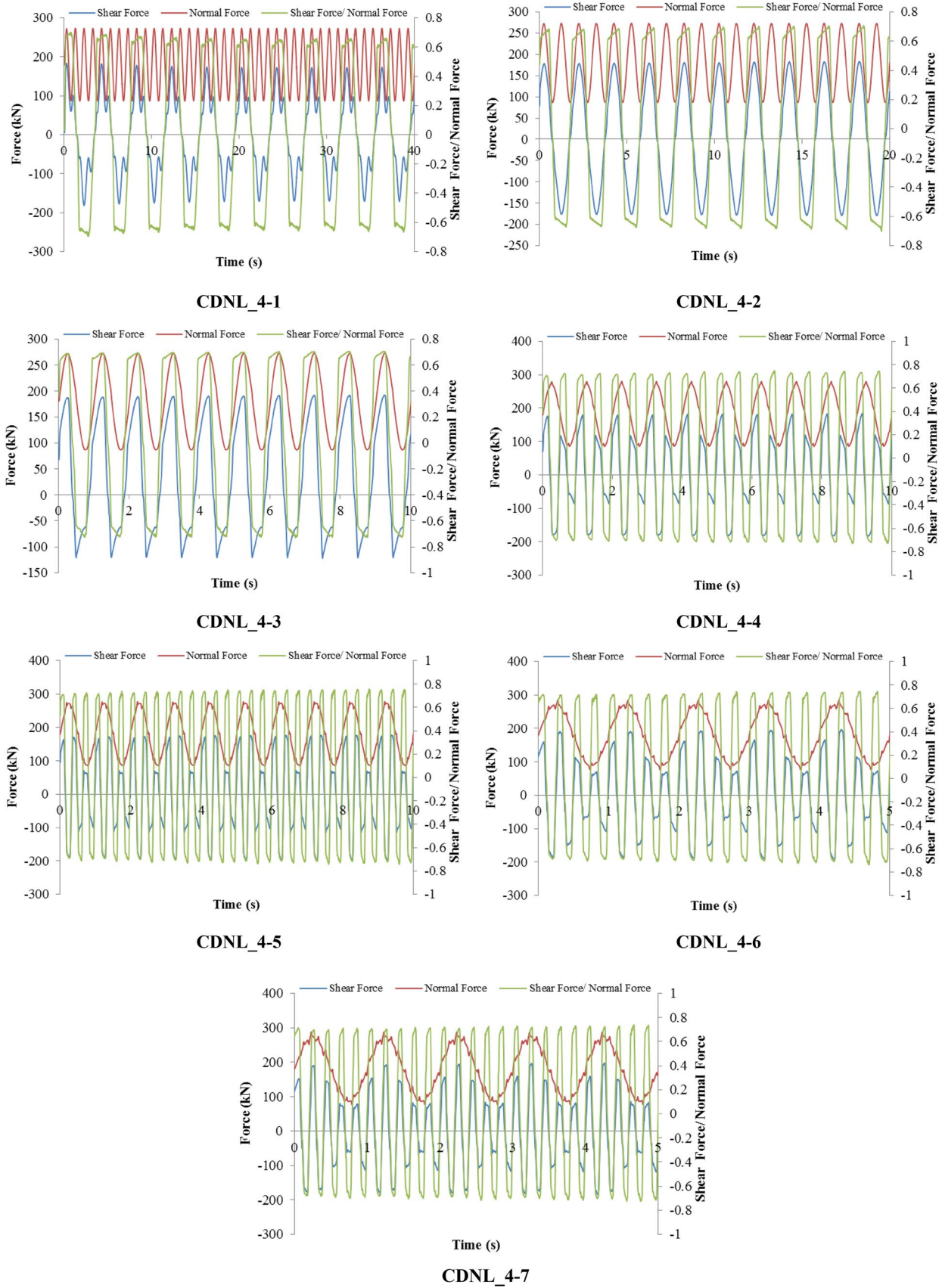
CDNL_2-1

CDNL_2-2

CDNL_2-3

CDNL_2-4

CDNL_2-5

CDNL_2-6

Fig. 19 (continued)

CDNL_3-1

CDNL_3-2

CDNL_3-3

CDNL_3-4

CDNL_3-5

CDNL_3-6

CDNL_3-7

Fig. 19 (continued)

CDNL_4-1

CDNL_4-2

CDNL_4-3

CDNL_4-4

CDNL_4-5

CDNL_4-6

CDNL_4-7

Fig. 19 (continued)

CDNL_5-1

CDNL_5-2

CDNL_5-3

CDNL_5-4

CDNL_5-5

CDNL_5-6

CDNL_5-7

Fig. 19 (continued)

CDNL_6-1

CDNL_6-2

CDNL_6-3

CDNL_6-4

CDNL_6-5

CDNL_6-6

CDNL_6-7

Fig. 19 (continued)

CDNL_7-1

CDNL_7-2

CDNL_7-3

CDNL_7-4

CDNL_7-5

CDNL_7-6

Fig. 19 (continued)

CDNL_8-1

CDNL_8-2

CDNL_8-3

CDNL_8-4

CDNL_8-5

CDNL_8-6

Fig. 19 (continued)

CDNL_9-1

CDNL_9-2

CDNL_9-3

CDNL_9-4

CDNL_9-5
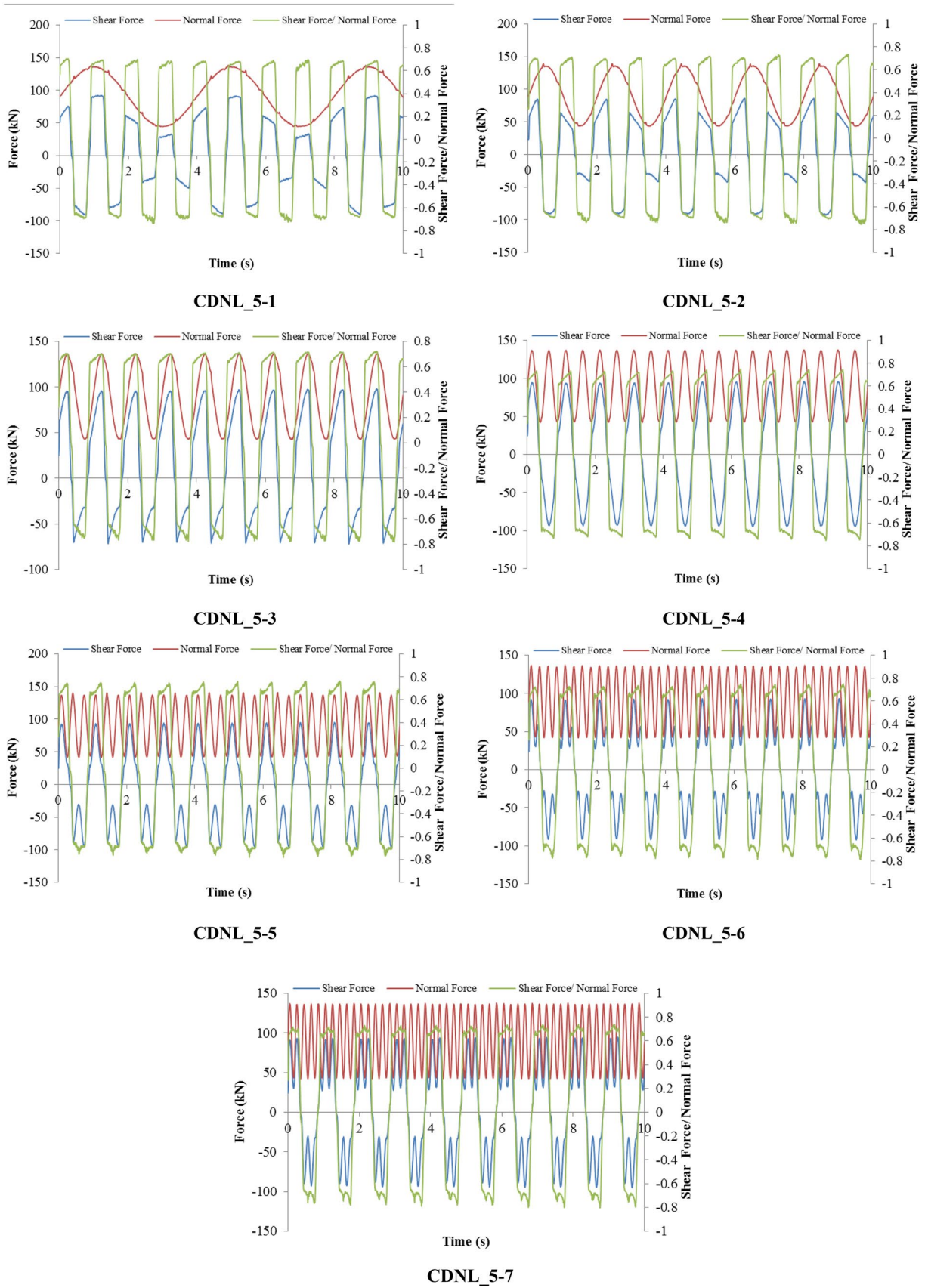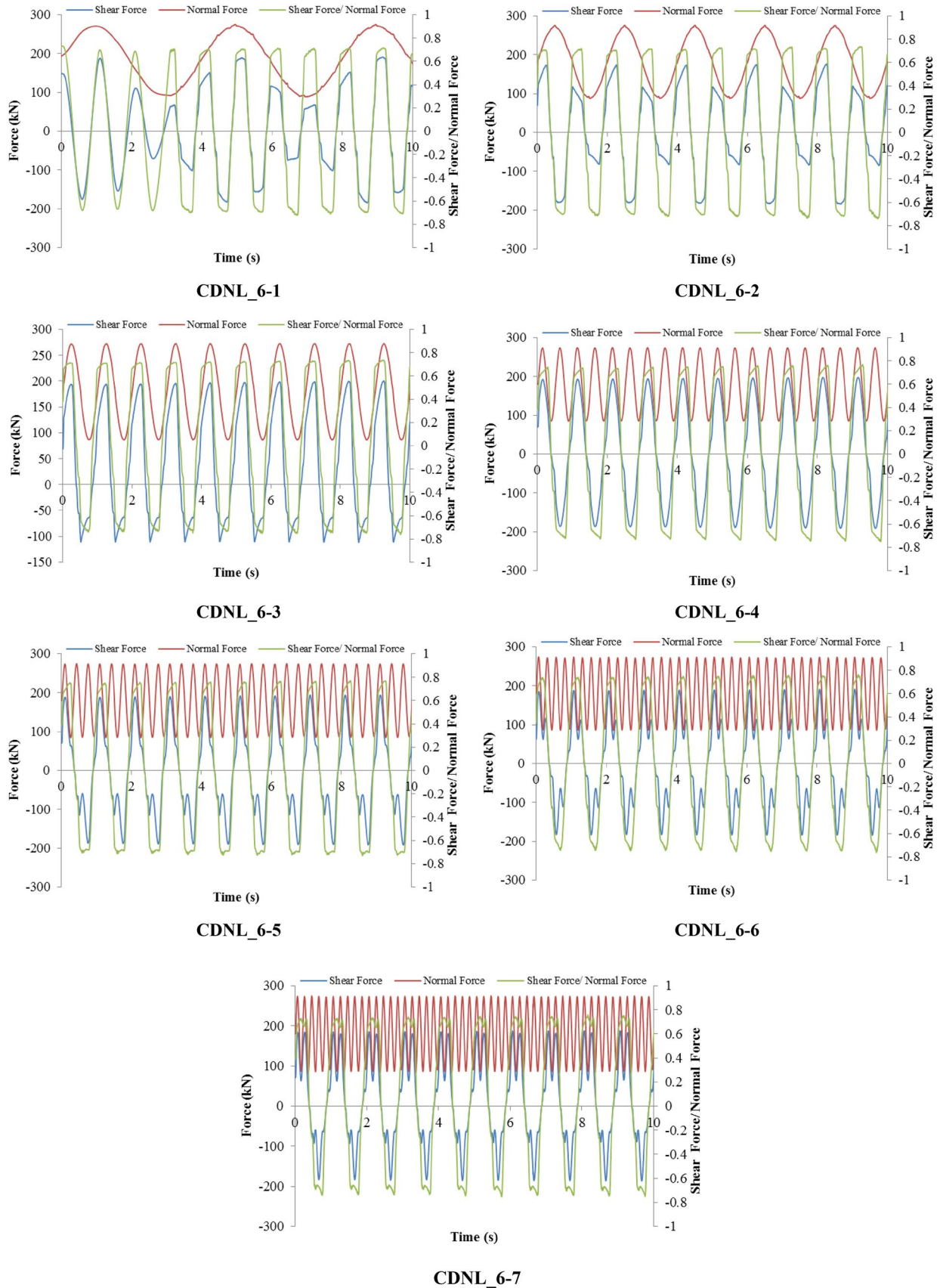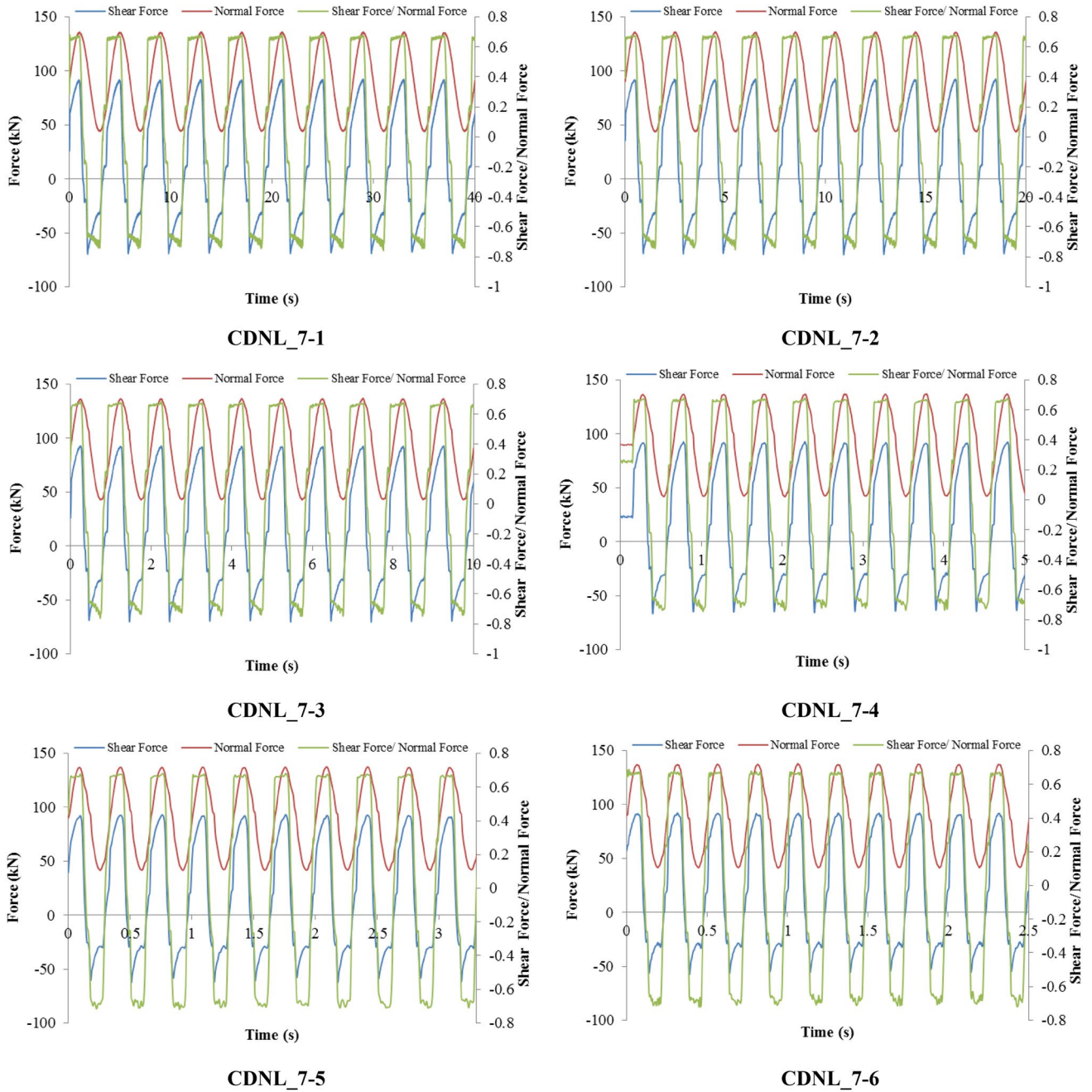
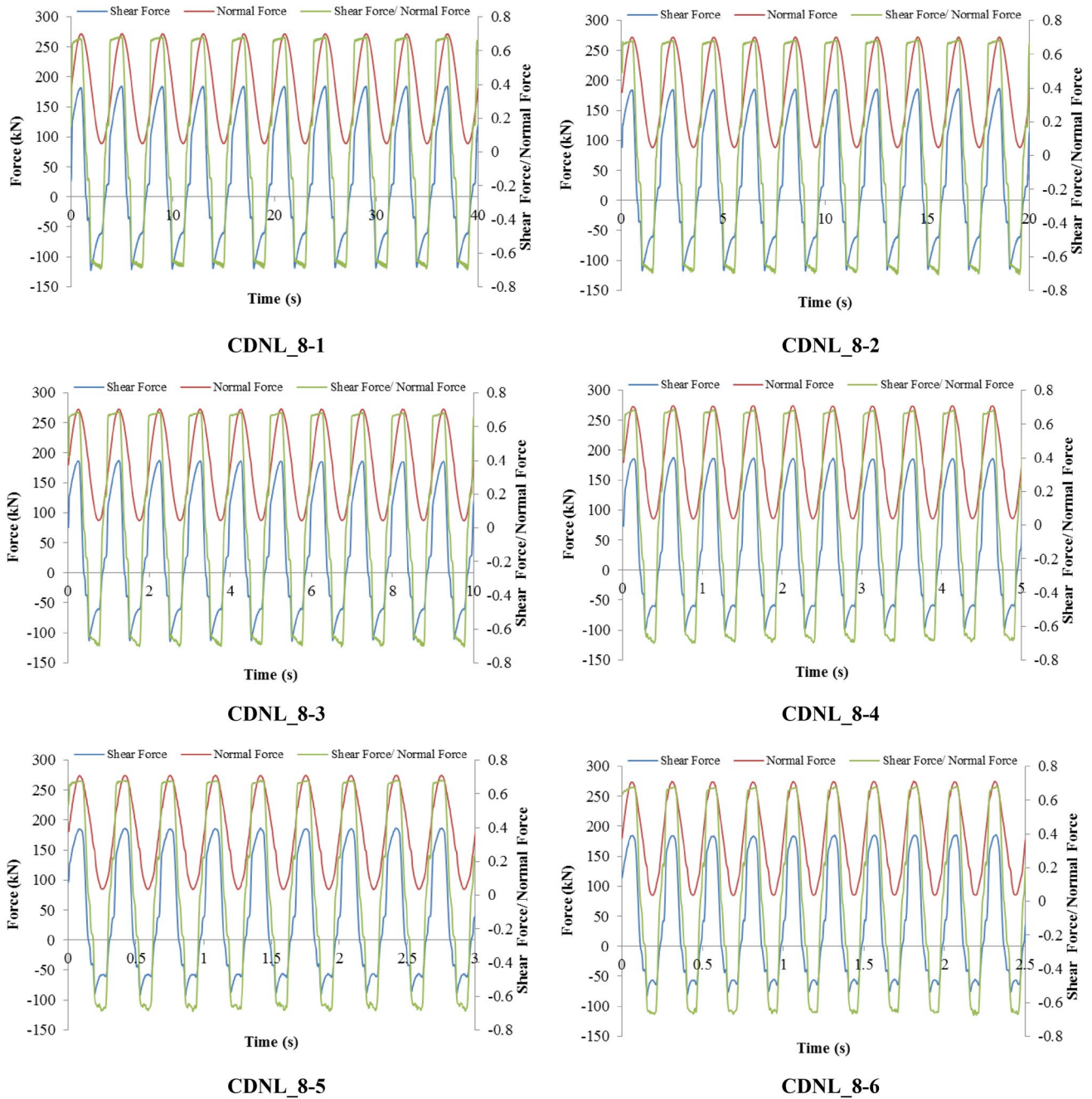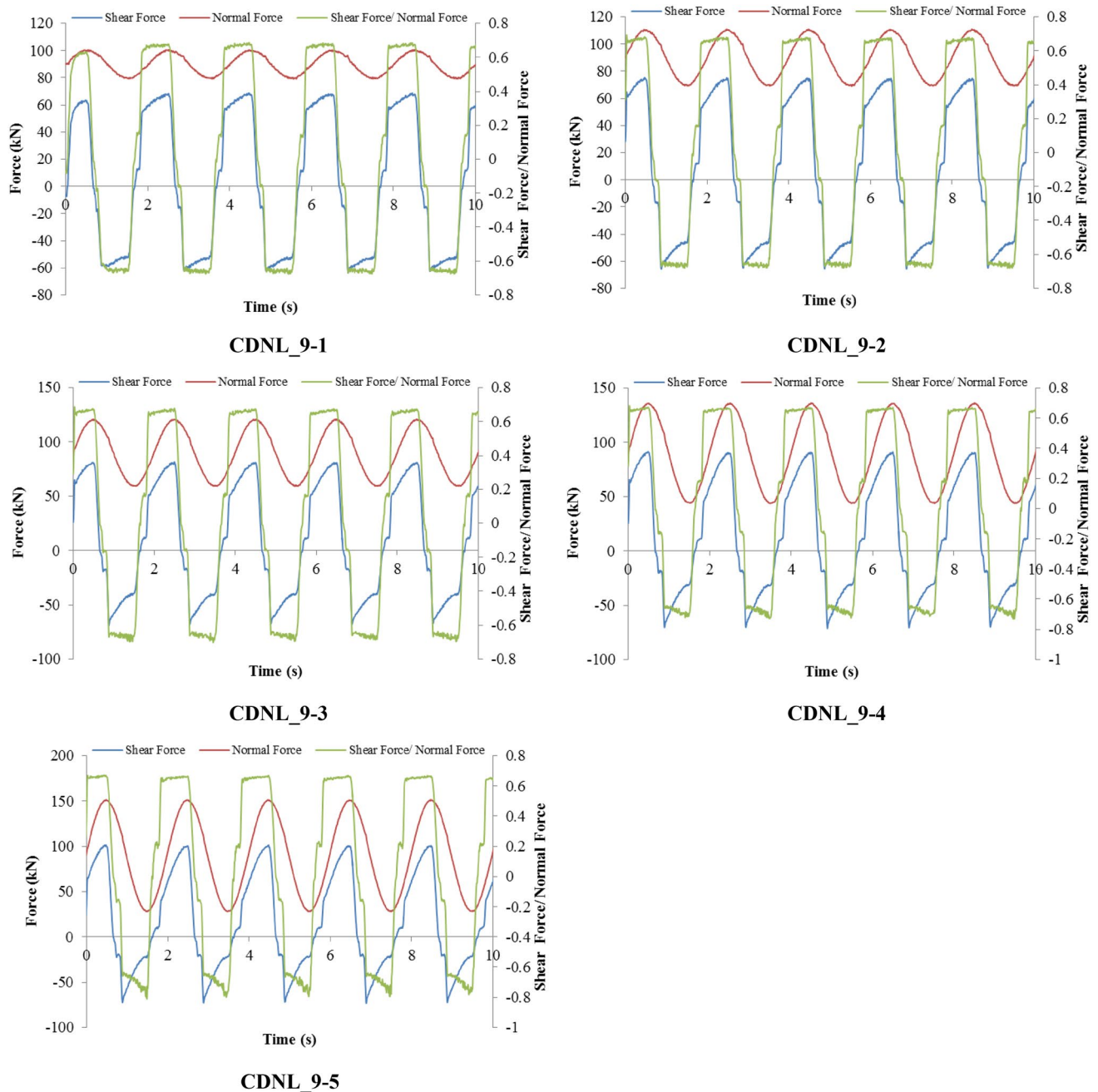**Fig. 19** (continued)

References

Bagde MN, Petros V (2005) Waveform effect on fatigue properties of intact sandstone in uniaxial cyclical loading. Rock Mech Rock Eng 38:169–196

Bochner S, Chandrasekharan K (1949) Fourier transforms. Princeton University Press, Princeton

Dang W, Konietzky H, Frühwirt T (2016a) Shear behaviour of a plane joint under dynamic normal load (DNL) conditions. Eng Geol 213:133–141

Dang W, Konietzky H, Frühwirt T (2016b) Rotation and stress changes of a plane joint during direct shear tests. Int J Rock Mech Min Sci 89:129–135

Dang W, Frühwirt T, Konietzky H (2017a) Behaviour of a plane joint under horizontal cyclic shear loading. Geomech Eng 13(5):809–823

Dang W, Konietzky H, Frühwirt T (2017b) Direct shear behavior of planar joints under cyclic normal load conditions: effect of different cyclic normal force amplitudes. Rock Mech Rock Eng 50(4):1–7

Dang W, Konietzky H, Herbst M, Frühwirt T (2017c) Complex analysis of shear box tests with explicit consideration of interaction between test device and sample. Measurement 102:1–9

Dang W, Konietzky H, Chang L, Frühwirt T (2018) Velocity-frequency-amplitude-dependent frictional resistance of planar joints under dynamic normal load (DNL) conditions. Tunn Undergr Space Technol 79:27–34

Dang W, Wu W, Konietzky H, Qian J (2019) Effect of shear-induced aperture evolution on fluid flow in rock fractures. Comput Geotech 114:103152

Fathi A, Moradian Z, Rivard P, Gérard B (2016) Shear mechanism of rock joints under pre-peak cyclic loading condition. Int J Rock Mech Min Sci 83:197–210

Ferrero AM, Migliazza M, Tebaldi G (2010) Development of a new experimental apparatus for the study of the mechanical behaviour of a rock discontinuity under monotonic and cyclic loads. Rock Mech Rock Eng 43:685–695

Guo YT, Zhao KL, Sun GH, Yang CH, Hong-Ling MA, Zhang GM (2011) Experimental study of fatigue deformation and damage characteristics of salt rock under cyclic loading. Rock Soil Mech 32:1353–1359

Hobbs BE, Brady BHG (1985) Normal stress changes and the constitutive law for rock friction. Eos Trans AGU 66:385 **(abstract)**

Hong T, Marone C (2005) Effects of normal stress perturbations on the frictional properties of simulated faults. Geochem Geophys Geosyst 6:1–17

Kilgore B, Lozos J, Beeler N, Oglesby D (2012) Laboratory observations of fault strength in response to changes of normal stress. J Appl Mech 79:031007

Kilgore B, Beeler NM, Lozos JD (2017) Oglesby, rock friction under variable normal stress. J Geophys Res Solid Earth 122:1–34

Konietzky H, Frühwirt T, Luge H (2012) A new large dynamic rockmechanical direct shear box device. Rock Mech Rock Eng 45(3):427–432

Lee HS, Park YJ, Cho TF, You KH (2001) Influence of asperity degradation on the mechanical behavior of rough rock joints under cyclic shear loading. Int J Rock Mech Min Sci 38:967–980

Li X, Tao M, Wu C, Du K, Wu Q (2017) Spalling strength of rock under different static pre-confining pressures. Int J Impact Eng 99:69–74

Linker MF, Dieterich JH (1992) Effects of variable normal stress on rock friction: observations and constitutive equations. J Geophys Res 97:4923–4940. https://doi.org/10.1029/92JB00017

Liu Z, Dang W (2014) Rock quality classification and stability evaluation of undersea deposit based on M-IRMR. Tunn Undergr Space Technol 40(2):95–101

Liu EL, He SM, Xue XH (2011) Dynamic properties of intact rock samples subjected to cyclic loading under confining pressure conditions. Rock Mech Rock Eng 44:629–634

Liu EL, Huang RQ, He S (2012a) Effects of frequency on the dynamic properties of intact rock samples subjected to cyclic loading under confining pressure conditions. Rock Mech Rock Eng 45:89–102

Liu Z, Dang W, He X (2012b) Undersea safety mining of the large gold deposit in Xinli District of Sanshandao Gold Mine. Int J Miner Metall Mater 19(7):574–583

Liu Z, Dang W, He X et al (2013) Cancelling ore pillars in large-scale coastal gold deposit: a case study in Sanshandao gold mine, China. Trans Nonferr Met Soc China 23(10):3046–3056

Marone C (1998) Laboratory-derived friction laws and their application to seismic faulting. Annu Rev Earth Planet Sci 26(1):643–696

Mirzaghorbanali A, Nemcik J, Aziz N (2014) Effects of shear rate on cyclic loading shear behaviour of rock joints under constant normal stiffness conditions. Rock Mech Rock Eng 47:1931–1938

Molinari A, Perfettini H (2017) A micromechanical model of rate and state friction: 2. effect of shear and normal stress changes. J Geophys Res Solid Earth 122:2638–2652

Olsson WA (1988) The effects of normal stress history on rock friction, key questions in rock mechanics. In Proceedings of the 29th US Symposium, edited by PA Cundall, RL Sterling, AM Starfield, University of Minnesota, Balkema, pp 111–117

Osei Tutu A, Steinberger B, Sobolev SV, Rogozhina I, Popov AA (2017) Effects of upper mantle heterogeneities on lithospheric stress field and dynamic topography. Solid Earth Discuss. https://doi.org/10.5194/se-2017-111 **(in review)**

Rice JR (2006) Heating and weakening of faults during earthquake slip. J Geophys Res 111:B05311

Song Z, Frühwirt T, Konietzky H (2018) Characteristics of dissipated energy of concrete subjected to cyclic loading. Constr Build Mater 168:47–60

Stein RS (1999) The role of stress transfer in earthquake occurrence. Nature 402(6762):605–609

Tiwari AK, Singh A, Eken T, Singh C (2017) Seismic anisotropy inferred from direct *S*-wave-derived splitting measurements and its geodynamic implications beneath southeastern Tibetan Plateau. Solid Earth 8:435–452. https://doi.org/10.5194/se-8-435-2017

Zhou Z, Wu Z, Li X (2015) Mechanical behavior of sandstone under cyclic point loading. Trans Nonferr Met Soc China 25:2708–2717

Zhou Z, Tan L, Cao W (2017) Fracture evolution and failure behaviour of marble specimens containing rectangular cavities under uniaxial loading. Eng Fract Mech 184:183–201

Zhou Z, Zhao Y, Cao W et al (2018) Dynamic response of pillar workings induced by sudden pillar recovery. Rock Mech Rock Eng 51:3075–3090